THE ASTROPHYSICAL JOURNAL, 196: 51–72, 1975 February 15

THEORY OF PULSARS: POLAR GAPS, SPARKS, AND COHERENT MICROWAVE RADIATION

M. A. RUDERMAN*
AND
P. G. SUTHERLAND†
Department of Physics, Columbia University
Received 1974 April 29; revised 1974 July 8

ABSTRACT

The huge magnetic fields characteristic of pulsars cause the nuclei (largely iron) of the stellar surface to form a tightly bound condensed state. Except for the very young Crab pulsar, theory and observation both support the view that the stellar surface is not hot enough to sustain an outflow of positive ions to balance the outflow of electrons as charge leaves the magnetosphere through the light cylinder along the open magnetic field lines. Adopting the conventional assumption that electrons do not return to the neutron star by coming back through the light cylinder along the open field lines, we are led to the following consequences for a neutron star whose magnetic moment tends to be antiparallel (as opposed to parallel) to its spin angular momentum: A polar magnetospheric gap is formed that spans the open field lines from the stellar surface up to an altitude of about 10^4 cm. In the gap $\boldsymbol{E}\cdot\boldsymbol{B} \neq 0$, although it vanishes essentially everywhere else in the near magnetosphere. The potential difference between the base and top of the gap is about 10^{12} volts. The gap continually breaks down (sparking) by forming electron-positron pairs on a time scale of a few microseconds. The gap positrons move out along the open field lines, and electrons flow to the stellar surface to close the pulsar's homopolar generator circuit as in the related Sturrock model.

We show how this can lead to injection into the near magnetosphere of ultrarelativistic positrons and the pairs subsequently produced by curvature radiation from the positrons leads to coherent microwave radiation in the frequency range and with remarkably many of the characteristics observed in pulsars. The properties and energetics of the sparking in the gap lead directly to (i) the maximum total luminosity of the pulsar and its dependence on period P: $L_{\max} \sim 10^{30} P^{-15/7}$ ergs s^{-1}, (ii) the observed drifting of subpulses and quantitative expressions for P_2 and P_3 (assuming that the sparking is localized, rapidly fluctuating but only rarely self-quenching), (iii) microstructure of pulses, (iv) the turnoff of a pulsar as its period increases, and (v) apparent weakening of the magnetic field in older pulsars. The production of coherent microwave radiation in the near magnetosphere results in substantial qualitative agreement with observations in these areas: (i) shapes and widths of pulse envelopes, (ii) their period and frequency dependence, and (iii) the sweep of linear polarization through the pulse envelope.

Subject heading: pulsars

I. INTRODUCTION

A spinning magnetized neutron star generates huge potential differences between different parts of its surface. Near the neutron star charged particles can flow only along magnetic field lines: since these lines do not cross, the pulsar circuits that utilize these potential differences are not completed near the star. Rather, charged particles flow out from the star to the neighborhood of the light cylinder (where the corotation velocity is the velocity of light). Here complete solutions for pulsar magnetospheres are not yet available, but it appears that there is mainly an outward flow of relativistic charged particles through the light cylinder. The open magnetic field lines which penetrate the light cylinder play a role analogous to that of conducting wires in ordinary circuits. If the wire is broken near the pulsar surface, the entire potential drop could be developed across the gap. Such a situation begins to arise at a pulsar surface out of which ions cannot be pulled by the electric field component parallel to the surface magnetic field $\boldsymbol{B}_s$.

This retention of ions, characteristic of a metal (solid or liquid), is a consequence of the huge surface magnetic field of a pulsar (except in the case of the very young Crab pulsar). The outflow of charged particles along field lines from the outer regions of the magnetosphere causes a magnetospheric gap to build up on the (open) field lines which connect it to the stellar surface; there $\boldsymbol{E}\cdot\boldsymbol{B}$ does not vanish as it essentially does everywhere else in the near magnetosphere. If not limited by a "breakdown" of the vacuum, the gap would grow until the entire available potential drop would develop along a field line traversing the gap. But before the gap grows to this extent, the region within the gap becomes unstable against the avalanche growth of electron-positron pairs. This occurs when a potential drop across the gap of close to 10^{12} V is reached. For most pulsars the breakdown gap width is about 10^4 cm. The electron-positron "sparking" provides the necessary positive charge to close the pulsar circuit as gap electrons flow back to the surface and keep the gap from growing. The maximum value

* Research supported by NSF grant GP-32336x.
† Research supported in part by NSF grant GP-32336x and in part by AEC grant AT (11-1)-2271.

of the electric field component along $\boldsymbol{B}_s$, reached just as a spark begins to grow, is generally many orders of magnitude less than that necessary to pull appreciable currents of positive ions from the stellar surface. In a similar model Sturrock (1971) considered electron-positron production from the curvature radiation of electrons (and protons) flowing out of the stellar surface. The accelerating electric fields were essentially taken as those which would obtain if there were no corotating magnetosphere at all on open field lines. The associated accelerating voltages are then much greater than those from space charge effects in the corotating magnetosphere associated with bringing the emitted electrons to relativistic speeds. These give (for a $P = 1$ s pulsar) less than a 10^{10} V potential drop above the surface (Michel 1974); this is much too low for subsequent curvature radiation to support electron-positron production.

Once the positrons leave the relatively small (10^4 cm) gap, they are in a region where $\boldsymbol{E}\cdot\boldsymbol{B} = 0$ and are no longer significantly accelerated parallel to $\boldsymbol{B}$ until they reach or penetrate the light cylinder. They move along curved field lines in a region of the magnetosphere whose angular rotation differs from that of the star. (Only if $\boldsymbol{E}\cdot\boldsymbol{B} = 0$ all along a segment of a magnetic field line will charged particles on that segment corotate with each other; corotation with the star itself follows only if that segment extends to the stellar surface.) The curvature radiation from these positrons considerably beyond the gap will produce electron-positron pairs just as it did in the gap. These secondary particles are argued to bunch appropriately to give coherent microwave radiation, a remarkable number of whose properties are coincident with those observed in pulsars. The significance of electron-positron production from curvature radiation near the surface of a pulsar has already been pointed out by Sturrock (1971), a number of whose seminal ideas are supported in the model we shall deduce.

Most of the features of this radiation are apparent in the simplified geometry in which an axisymmetric pulsar magnetic field is parallel or antiparallel to its spin axis (Goldreich and Julian 1969). In § II we begin with a brief review of some of the features of the standard model in which charges of both signs can flow freely from the stellar surface. Of special interest will be those neutron stars whose magnetic moment is directed antiparallel to their spin angular momenta so that the corotating magnetosphere plasma above the polar caps has a net positive charge. Section III summarizes the arguments for believing that, except in the case of the Crab pulsar, a pulsar surface will not be an emitter of positive ions even though electrons may come easily from the surface. Here the special nature of matter in a superstrong (10^{12} gauss) magnetic field is crucial. Section IV and the Appendix consider the consequences for the near magnetosphere of a spinning neutron star when charges flow out through the light cylinder, but are not replaced by an equivalent flow of charge out from the stellar surface. The inability of the stellar surface to supply a flow of positive ions ultimately causes the near magnetosphere above the polar cap to pull away from the surface and leave a gap. In this gap $\boldsymbol{E}\cdot\boldsymbol{B}$, which essentially vanishes everywhere else in the near magnetosphere and within the neutron star, differs from zero by an amount roughly proportional to the gap height h. A potential drop proportional to h^2 develops along the magnetic field lines in the gap; test particles in the gap and the magnetosphere along the open field lines above it no longer corotate with the star and the rest of the magnetosphere.[1] Section V shows that the gap height h and the potential difference between its top and bottom will be limited by the onset of an instability in which sparks discharge across the gap. The formation of an electron-positron discharge in the gap occurs when the potential difference reaches about 10^{12} V. Then charged particles accelerated in the gap and moving along curved magnetic field lines produce curvature radiation with photon energy sufficiently greater than $2m_ec^2$ that these photons can produce e^--e^+ pairs on neighboring field lines. Further energetic radiation will be produced, and this can go on to produce more pairs and so on. Through this cascade process the gap can be discharged by an electron-positron spark as electrons flow to the pulsar surface and positrons move out along open field lines to the light cylinder. We determine the thickness h of the gap to be that for which a quasi-stable discharge is attained, and find $h \sim 5 \times 10^3$ cm for a $P = 1$ s pulsar with magnetic field $B \sim 10^{12}$ gauss. Section VI considers some special properties of polar gap sparks which will have direct observational consequences for the coherent microwave radiation they will ultimately cause in the plasma beyond the gap. Sparks feed relativistic positron beams into localized bundles of open field lines. These sparks are shown to drift around the polar gap with a period P_3 whose magnitude and dependence on the neutron star's rotation period agree well with that observed for drifting subpulses (Backer 1973). The expected spacing between sparks in the gap corresponds to and fits the observed subperiod P_2. Growth, persistence, and partial decay of sparks last a few microseconds. At the beginning of a spark, injected positrons have $\gamma \sim 3 \times 10^6$; this is expected to drop sharply at the very end of the spark as the gap potential drop is shorted by the separation of the large e^- and e^+ densities which have been produced in the discharge. This drop in injected positron energies is significant for details of the subsequent coherence of microwave radiation. Section VII considers the complete absence of sparking in pulsars whose period P exceeds $P_{\rm crit} = 1.7(B_s^d/10^{12})^{8/13}$ seconds, where B_s^d is the surface component of the dipole magnetic field. In this limit our model coincides with that of Sturrock except for the description of the surface magnetic field. It gives a cutoff in observable pulsar periods very near that observed. A further consequence is shown to be a good fit to the observed distribution of $(P\dot{P})^{1/2}$ with pulsar age which has also been attributed to a decrease in the pulsar magnetic field with age (Gunn and Ostriker 1970).

[1] See note added in proof.

In § VIII it is shown how the outflowing positrons from the gap will convert a substantial fraction of their kinetic energy ($\sim 10^{30} P^{-15/7}$ ergs s^{-1}) into coherent microwave radiation. Positrons created near the beginning of the spark have extreme relativistic energies corresponding to $\gamma \sim 3 \times 10^6$. Immediately above the gap there is no further acceleration, but curvature radiation such as that which initiated the spark in the 10^4 cm gap continues. Conversion of these gamma rays in the region above the gap fills it with an e^--e^+ plasma. Near the star the magnetic field is presumed to be described by many multipoles in a complicated way, but with a characteristic radius of curvature of field lines comparable to the stellar radius. Then the conversion is very efficient for pair creation within about 10^6 cm of the stellar surface. These pairs have an energy of $2\gamma_\pm mc^2$ with $\gamma_\pm \simeq 800$. The number density of these pairs is $\sim 3 \times 10^6/\gamma_\pm \sim 4 \times 10^3$ greater than that of the spark positrons or that of the charge-separated plasma needed for corotation. Although unaccelerated by electric fields, these pairs move out at speed c along the curved open field lines (with a momentum along the field equal to that of the momentum component of the photon that produced them). They of course also produce curvature radiation; but because $\gamma_\pm \simeq 800$ and, to a much lesser extent, because the radius of curvature of the field lines is rapidly increasing as the pairs move away from the neutron star into an essentially pure dipole region, the curvature radiation falls in the radio band. The efficiency of incoherent single-particle radiation is negligibly small, but bunching of the particles in the plasma would make the conversion of the kinetic energy of the pairs into curvature radiation vastly more efficacious. An effective bunching mechanism is provided by the streaming of the much more energetic spark-gap–accelerated positrons through this pair plasma. The induced bunching of charge in this plasma by the classical two-stream instability with a relativistic beam is considered in § VIII. Bunching of the required magnitude and with the appropriate spatial and time scales to give strong coherent radiation is calculated to begin where the pair-plasma frequency beyond the gap passes below the characteristic frequency of curvature radiation from this same plasma. This occurs much farther from the neutron star as its period increases and can extend to distances $\sim 10^8$ cm in the oldest pulsars. The fundamental role of curvature radiation of the secondary electron-positron pairs in giving pulsar microwave radiation is just that proposed by Sturrock (1971) and Tademaru (1971). Details of the bunching and of the geometrical regime involved are quite different.

Section IX compares theory and observation for pulse properties. In older pulsars the coherent radiation comes mainly from a distant toroidal region whose center is hollowed by negligible field curvature. Since the coherent radiation is emitted essentially tangent (within $\gamma_\pm^{-1}$) to the magnetic field lines, a distant observer passing through the radiated beam would see mainly a two-humped structure for an integrated pulse profile if, on the average, sparks fill all parts of the gap with equal probability. For shorter-period pulsars the dimensions of the hollowed center of the radiation region are much reduced, and it is expected that a two-humped pulse profile is less likely to be observed for these pulsars. Calculated period and frequency dependence of the pulse shapes agrees reasonably with observations. The continuous sweep of linear polarization through the pulse envelope, typical of most pulsars (see, for example, Manchester 1971), is readily understood in terms of the dipole structure of the magnetic field in the near magnetosphere, as first proposed by Radhakrishnan and Cooke (1969). Observational support for near-magnetosphere emission, based on pulse structure and polarization, has been summarized in the past by Manchester (1971), ter Haar (1972), and Manchester *et al.* (1973).

II. THE STANDARD MODEL: DEFINITIONS

Goldreich and Julian (1969) elucidated the characteristics of the corotating magnetosphere surrounding an axisymmetric neutron star with aligned magnetic moment and rotation axes. They assumed that (*a*) the neutron star can supply the necessary negative charges (electrons) and positive charges (ions and positrons) required to fill and maintain the magnetosphere with $\boldsymbol{E}\cdot\boldsymbol{B} \sim 0$, and (*b*) the currents in the magnetosphere are negligible. They showed that the magnetosphere would then corotate with a local charge density

$$\rho_e = -\frac{\boldsymbol{\Omega}\cdot\boldsymbol{B}}{2\pi c}\frac{1}{1 - \Omega^2 r_\perp^2/c^2} \tag{1}$$

where $r_\perp = r \sin\theta$ and θ is the polar angle. With the charge density of equation (1), the electric field in the neutron star and in its magnetosphere vanish in a corotating reference frame. In the stationary observer's frame

$$\boldsymbol{E} = -(\boldsymbol{\Omega} \times \boldsymbol{r}) \times \boldsymbol{B}/c\,. \tag{2}$$

In that approximation which neglects the magnetic field contribution from magnetospheric currents, the magnetic field far from the neutron star surface is dominated by the star's own dipole field. Those field lines which originate sufficiently close to the stellar polar caps will cross the light cylinder of radius

$$R_c \equiv c/\Omega \tag{3}$$

at which exact corotation can no longer be maintained. These open field lines will define two "polar caps" on the stellar surface from which charged particles leaving the star can move along field lines and escape from the corotating magnetosphere by passing through the light cylinder. At the light cylinder the "corotating" magnetosphere carries one sign of net charge along an equatorial belt and the opposite sign above and below it (cf. fig. 1). A (centrifugally induced) loss of charged particles out through the light cylinder would cause $\boldsymbol{E}\cdot\boldsymbol{B} \neq 0$. To continually restore it, a current of each sign would flow out from regions of the polar caps as sketched in figure 1. In the original model of Goldreich and Julian (1969) an outward negative (positive)

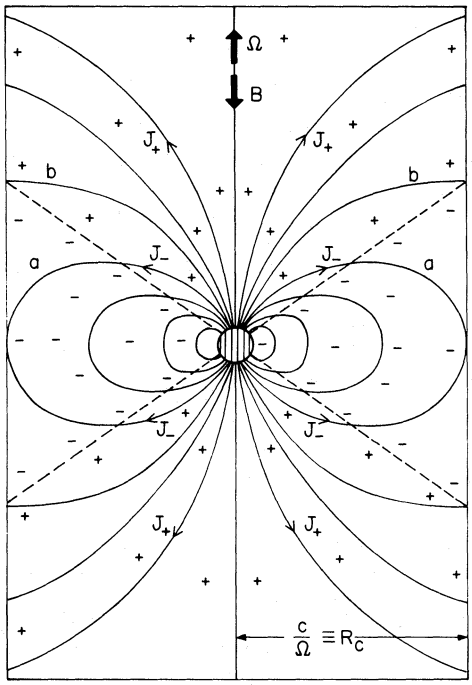

FIG. 1.—Sketch of the magnetic field lines, currents, and magnetospheric charge density for a Goldreich and Julian (1969) model in which the rotation axis and magnetic dipole axis are antiparallel. The magnetic field is assumed to be purely dipolar. The dashed lines, at $\cos\theta = \pm 3^{-1/2}$, separate the magnetospheric regions of positive and negative charge density with $\rho_e = -\boldsymbol{\Omega}\cdot\boldsymbol{B}(2\pi c)^{-1}$. From the equator to the pole: Line *a* is the last field line to close within the light cylinder ($R_c = c\Omega^{-1}$); Lines between *a* and *b* are open and pass through regions of negative charge as they penetrate the light cylinder; negative currents (J_-) flow along these lines from the star. The open magnetic field lines between line *b* and the pole pass through regions of positive charge, and positive currents (J_+) flow along them.

charge flow is presumed to exist, even through a net positively (negatively) charged polar magnetosphere. In other models (Michel 1974) it is presumed that the magnetosphere charge above an emitting region must match that of the outflowing charge. Detailed computations (Kuo-Petravic, Petravic, and Roberts 1974) suggest the further complication of some field line crossing and backflow into the star to balance the outflow from the polar region. We shall consider, in this paper, mainly spinning neutron stars whose magnetic moments are *antiparallel* to their spins, i.e., those for which the magnetosphere just above the polar caps has a net *positive* charge. These we shall call pulsars. If the spin and moment are parallel so that the magnetosphere above the polar caps is negative, we shall use the designation *antipulsar*, although we shall not consider in this paper possible radiation mechanisms for antipulsars. For pulsars the gap formed above the polar cap does not depend on the detailed way in which electrons leave the star elsewhere or positive particles return to it; this may not be true for antipulsars.

In the pure dipole field approximation for a pulsar, the radius of the polar cap region out of which a net flow of positive charges is needed to maintain the magnetosphere is

$$r_{p_+}{}^d = \left(\frac{2}{3}\right)^{3/4} R\left(\frac{\Omega R}{c}\right)^{1/2} \approx 10^4 P^{-1/2}\ \text{cm}\,, \qquad (4)$$

where R is the stellar radius. The outer radius to the foot of the last open field line of figure 1 is

$$r_{p_-}{}^d = R\left(\frac{\Omega R}{c}\right)^{1/2} \approx 1.4 \times 10^4 P^{-1/2}\ \text{cm}\,, \qquad (5)$$

where P is the rotation period and $R \sim 10^6$ cm. In the Goldreich and Julian model, negative currents flow from an annulus between essentially r_{p_+} and r_{p_-}. The net magnetic flux through the polar cap region within $r_{p_+}{}^d$ is

$$\Phi_+ = \pi(r_{p_+}{}^d)^2(\boldsymbol{B}_s{}^d\cdot\hat{r})\,, \qquad (6)$$

where $\boldsymbol{B}_s{}^d$ is the surface component of the dipole field at the polar cap. For a more realistic pulsar, many multipoles contribute to the near field of the neutron star, and the cap radii and field strengths are not determined by extrapolating in along the distant open field lines for which only the dipole component is important. However, the combination

$$\pi(r_p)^2(\boldsymbol{B}_s\cdot\hat{r}) \equiv \Phi\,, \qquad (7)$$

which gives the total flux penetrating the light cylinder, is unchanged by the removal of the dipole superscript d because $R_c \gg R$. In equation (7) $\boldsymbol{B}_s$ is the actual surface field strength. In very many of our applications it is just this combination of parameters that is relevant.

Thus, for example, from equation (2) it follows that the potential difference between the center of the polar cap and the edge of the negative current emission region is

$$\Delta V \approx \frac{\Omega(r_{p_-})^2}{2c}\,\boldsymbol{B}_s\cdot\hat{r} \approx \frac{\Omega}{2\pi c}\,\Phi\,, \qquad (8)$$

so that it can be expressed directly in terms of equations (4), (5), and (6) as

$$\Delta V \approx \frac{\Omega^2 R^3}{2c^2}\,(\boldsymbol{B}_s{}^d\cdot\hat{r}) \approx 6.6 \times 10^{12} B_{12}/P^2\ \text{volts} \qquad (9)$$

almost independent of the contribution of other multipoles to $\boldsymbol{B}_s$. In equation (9), B_{12} is the surface *dipole* component in units of 10^{12} gauss. It is this homopolar generator potential difference that can, in principle, ultimately be brought to bear across any gap or inertial drag which tends to restrict the outward flow of current along the open field lines. Although the above assumes $\boldsymbol{E}\cdot\boldsymbol{B} = 0$, and negligible particle streaming, the description is not expected to be greatly altered (Michel 1974) by current flow, especially near the star which will be our main region of concern.

The maximum net charged-particle flux from the polar cap is, from equation (1),

$$\dot{N}_{\max} \approx \pi r_p^2 \frac{\boldsymbol{\Omega}\cdot\boldsymbol{B}_s}{2\pi ec} c \approx \frac{\Phi\Omega}{2\pi e} . \quad (10)$$

This current flows beneath the stellar surface between the negative and positive emission regions of the polar caps. Because it must cross field lines to do this, it exerts a braking torque on the spinning star and reduces the stellar rotational energy at a rate

$$\frac{dE}{dt} \approx \frac{e\dot{N}B_s r_p^2\Omega}{c} \approx \frac{(B_s^d)^2\Omega^4 R^6}{c^3} . \quad (11)$$

This energy loss of $e\Delta V$ per net charged particle flowing through the surface is ultimately reflected in the acceleration (including overcoming space-charge impedance) of particles along the open field lines; most of this has been presumed to occur close to or beyond the light cylinder. However, the total rate of pulsar energy loss is completely determined by the current flowing out of the polar cap together with the surface magnetic field. An alternative derivation of equation (11), based on the magnetic torque at the light cylinder induced by the shearing of the magnetic field by the outflowing currents, has been given by Goldreich and Julian (1969) and Sturrock (1971).

These maximal energy loss formulae, when equated to the stellar energy loss rate $-I\Omega\dot{\Omega}$, give the surface dipole field in terms of the calculated moment of inertia of a neutron star. A typical I of 5×10^{44} g cm^2 (Baym, Pethick, and Sutherland 1971) gives characteristic $B_s^d \approx 1\text{–}3 \times 10^{12}$ gauss (a value which seems to vary remarkably little among pulsars; cf. Ruderman 1972*a*, Greenstein 1972). Equation (11) gives $\dot{\Omega} \propto -\Omega^n$ with $n = 3$. The distribution of Ω and $\dot{\Omega}$ among pulsars suggests that, except in the Crab, $n \approx 3.4$, which suggests that the net current flow is less than the maximum, especially in the slower pulsars. We return to this point in § VII where the turnoff of pulsars is discussed.

III. BINDING OF POSITIVE IONS IN A NEUTRON STAR SURFACE

The model of § II presumes that, except for space charge effects associated with the need to bring finite-mass electrons and especially nuclei to relativistic velocities, substantial currents will flow from a stellar surface as soon as $\boldsymbol{E}\cdot\boldsymbol{B}$ departs slightly from zero. But this is not expected to be the case, in most pulsars, for the positive ions. Calculations (Ruderman 1972*b*; Chen, Ruderman, and Sutherland 1974) show that the structure of matter in the surface layer of neutron stars with $B \approx 10^{12}$ gauss is largely determined by the magnetic field: long molecular chains (with axis parallel to $\boldsymbol{B}$) are formed with the ions (composed of nuclei and some core electrons) distributed in a one-dimensional lattice along the chain and with an outer sheath of electrons. These chains strongly attach to each other laterally, mainly because of strong fringe fields. The result is an anisotropic very dense, very strongly bound form of condensed matter. Although just after formation a hot neutron star may have an outer layer of helium which has cooled too rapidly to fuse (Rosen and Cameron 1972), whatever helium can be lifted from the stellar polar cap by pulsar electric fields will have disappeared for pulsars older than a thousand years or so.

One expects the matter in the outer stellar layers to be mainly ^{56}Fe: molecular chains composed of iron in a field $B \approx 2 \times 10^{12}$ gauss have a binding energy per ion of ~ 14 keV and a lattice spacing $\sim 10^{-9}$ cm (the sheath electrons have a Fermi energy ~ 750 eV). Because of the high binding energy per ion, in the absence of discharges such as those discussed in § V the ions are not expected to be stripped from the surface and contribute significantly to pulsar surface currents for the following reasons:

i) The electric field required to pull ions from the chains is of order $E_0 \sim 14$ keV$/Z_c el$, where eZ_c is the ion charge and l is the interior chain lattice spacing: for typical parameters $E_0 \sim 10^{12}$ V cm^{-1}. Even in the absence of any screening magnetosphere, the maximum surface electric field is only

$$E_{\max} \approx 2\pi RB/Pc \approx 10^{11}/P \text{ V cm}^{-1} \quad (12)$$

with P the pulsar period. For most pulsars $E_{\max} \ll E_0$; however, with a magnetosphere present the surface electric fields are much reduced, and in the limit of a corotating magnetosphere the surface electric field in a corotating frame vanishes and field emission of ions is impossible.

ii) At a temperature T an estimate of the maximum ion particle flux $\mathscr{F}$ which can be emitted from the pulsar surface (ignoring space charge limitations) is

$$\mathscr{F}(T) \sim \frac{\rho_z}{m_z}\left(\frac{kT}{m_z}\right)^{1/2} \exp\left(-E_B/kT\right) , \quad (12')$$

where m_z is the ion mass ($\sim 10^{-22}$ g), E_B is the surface binding energy (~ 14 keV), and ρ_z is the density of matter in the surface layers, $\sim 6 \times 10^3$ g cm^{-3} for $B \approx 2 \times 10^{12}$ gauss (Chen *et al.* 1974). For this flux to supply the magnetospheric charged-particle loss along open field lines the temperature must exceed T_c where

$$\hat{Z}e\mathscr{F}(T_c) = \rho_z c \approx \frac{\Omega B_s}{2\pi} . \quad (12'')$$

At $kT \sim \frac{1}{2}$ keV, ions will be emitted in relatively low states of ionization because of the exceedingly tight binding of all atomic electrons in superstrong magnetic fields. Then equation (12″) gives $T_c \sim 6 \times 10^6$ ° K for $P = 1$ s, $B = 2 \times 10^{12}$ gauss, $\hat{Z} = 3$. To sustain such a temperature, an energy flux of $\sim 10^{23}$ ergs cm^{-2} s^{-1} must be supplied to the stellar surface to support its 2 keV X-ray emission.

If the entire surface of the neutron star were at or above the temperature T_c, the X-ray flux of 10^{36} ergs s^{-1} would be easily detected, and such pulsar X-ray sources are not observed. This agrees with theoretical

calculations of the expected cooling of neutron star surfaces (Tsuruta *et al.* 1972). The high Fermi energy caused by the superstrong magnetic field in the pulsar surface matter right up to the "edge" greatly increases the thermal conductivity of such matter. Therefore, the star should cool even faster than the rates given in existing calculations.

Ohmic heating from a current such as that of equation (10) through the surface layers is much too small to keep the cap at a temperature large enough to overcome ionic binding. Interior frictional heating from differential rotation between a neutron star crust and a superfluid interior (Greenstein 1971) is similarly greatly insufficient. Thus, both observational and theoretical arguments strongly suggest that pulsars are generally not hot enough to boil off ions (unless there is some special intense heat source just at the polar caps).

iii) In most pulsar theories, and in the model to be described below, electrons and positrons are accelerated to relativistic energies, and extremely energetic particles of one charge may strike the surface. Even a very close collision of a relativistic particle with an ion nucleus will not be sufficient to dislodge it: the maximum energy transferred in a close collision (corresponding to the electron/positron just skimming the nuclear surface of radius r_N) is $\Delta E_{\max} \approx (Ze^2/r_N c)^2/2m_z \approx 1$ keV: this energy transfer is independent of the energy of the (relativistic) electron/positron and is much less than the molecular binding energy.

The above arguments concerning the inability of pulsar surfaces to provide ions to fill and maintain the magnetosphere are not applicable to the singular case of the very young short-period pulsar in the Crab Nebula: surface regions of this pulsar are predicted to be hot enough to boil off ions; in addition, this pulsar may be young enough to still retain a surface layer of helium for which the molecular binding energy is much less than that of iron.

Electrons, on the other hand, can be pulled from the stellar surface much more readily than positive ions. Although the electron work function has not been calculated for matter in superstrong magnetic fields, it has been estimated to be more than an order of magnitude less than the positive ion binding. In addition, quantum-mechanical barrier penetration can greatly increase field emission currents (Ruderman 1972*a*). In the model discussed below, we shall adopt the extreme assumption that the neutron star surface yields no positive ions at all but does not limit the outward flow of electrons in response to an appropriately directed, but arbitrarily small, electric field. But as long as electrons can flow out much more readily than ions from the polar cap, even the quantitative results are not sensitive to the precise amount of electron flow impedance.

IV. THE POLAR GAP

We shall deduce consequences for the near magnetosphere from two circumstances: (i) We accept the conventional wisdom that electrons, which flow out through the light cylinder along swept-back magnetic field lines, do not easily flow back through the light cylinder into the corotating magnetosphere. (ii) The neutron star surface is a copious supplier of electrons, but not of positive ions.

If the magnetospheric plasma is not initially completely charge-separated, it can supply the star with both an inflow of negative charge to replace the electrons which leave it and an outflow of positive charge to resupply that lost through the light cylinder. But this cannot continue indefinitely. Ultimately, in response to the outflow of positive charge through the light cylinder, the positively charged magnetosphere at the surface of the star begins to pull away from the surface and produces a growing gap. Wherever the near magnetosphere charge density is nonzero, $\boldsymbol{E}\cdot\boldsymbol{B} = 0$. A component of $\boldsymbol{E}$ anchored on surface-bound net positive charge gives $\boldsymbol{E}\cdot\boldsymbol{B} \neq 0$ only in gaps where the magnetosphere density vanishes. We can exhibit exact solutions only for a few special cases. For example, if the stellar surface binds both negative and positive charges while the, by now, charge-separated magnetosphere loses charge from closed as well as open field lines, then a simple exact solution can be exhibited for an axisymmetric pure multipole magnetic field: In the Appendix a rotating magnetosphere is derived for a rotating neutron star with an aligned pure dipole magnetic field. It differs from the usual solution in that the magnetosphere charge density is given by equation (1), but its angular frequency (Ω) is less than that of the neutron star (Ω^*). The magnetosphere is separated from the star by a spherical gap of thickness h, and the two rotation speeds are related by

$$\frac{\Omega^*}{\Omega(h)} = \frac{3}{5}\left[\frac{(R+h)^2}{R^2} + \frac{2}{3}\frac{R^3}{(R+h)^3}\right] \qquad (13a)$$

$$= (1 + 3h^2/R^2) \qquad (h \ll R)\,. \qquad (13b)$$

For the dipolar magnetic field, the electric field and associated charge density in the magnetosphere are quadrupolar and exactly that of a normal magnetosphere rotating at Ω; in the neutron star, the electric field is $\boldsymbol{E} = -(\boldsymbol{\Omega}^* \times \boldsymbol{r}) \times \boldsymbol{B}/c$. The electric field in the intervening vacuum gap is complicated. Although $\boldsymbol{E}\cdot\boldsymbol{B} \neq 0$, it vanishes at the base of the magnetosphere. At the pole the gap electric field at the neutron star is normal to the stellar surface and is given by

$$E_p = \frac{2\Omega^* B}{c} h \qquad (h \ll R)\,; \qquad (14)$$

and the potential across the gap, at the pole, is

$$\Delta V = \frac{\Omega^* B}{c} h^2\,. \qquad (15)$$

(We have discovered no instability in the above gap solution.)

We emphasize that the usual demonstration of corotation for the magnetosphere of a rotating mag-

netized star fails in this case, and in general, if $\boldsymbol{E}\cdot\boldsymbol{B}$ does not vanish everywhere along magnetic field lines connecting the star and its magnetosphere (see the Appendix and Gold 1959).

A case of physical interest consists in the gap formed when positive charge flows out along the open field lines emanating from the polar cap of radius r_{p+} (fig. 1 and eq. [4]) and the surface binding of ions does not permit its replacement from the star. When the thickness of the gap $h \ll r_{p+}$, the relationship between h and the potential drop along a field line traversing the gap is the same as that of equation (15):

$$\Delta V = 2\pi\rho_e h^2 = \Omega^* B_s h^2 c^{-1} . \qquad (16)$$

In equation (16), ρ_e is the positive charge density, given by equation (1), which was in the gap region before the gap was formed and is now held by the surface. In this limit of very small h, $\boldsymbol{E}\cdot\boldsymbol{B}$ *above* the gap is therefore just what it was without the gap, i.e., zero. The geometrical structure of the gap is given schematically in figure 2: in addition to the gap $ab' = de' = h$, a gap also forms along the open field lines which pass the edge of the polar cap of radius r_{p+}. This separation $cc' \approx h$ also, except near the corner b'. In this part of the gap $\boldsymbol{E}$ and $\boldsymbol{B}$ are orthogonal so that $\boldsymbol{E}\cdot\boldsymbol{B} = 0$. Outside of the region *cbadef* the near magnetosphere and the star corotate like a rigid structure with angular frequency Ω^*. Within the isolated magnetosphere polar-column region $c'b'e'f'$ there is a variable $\Omega' < \Omega^*$, parallel to $\boldsymbol{\Omega}^*$ and constant along, but varying between, field lines (cf. the Appendix).

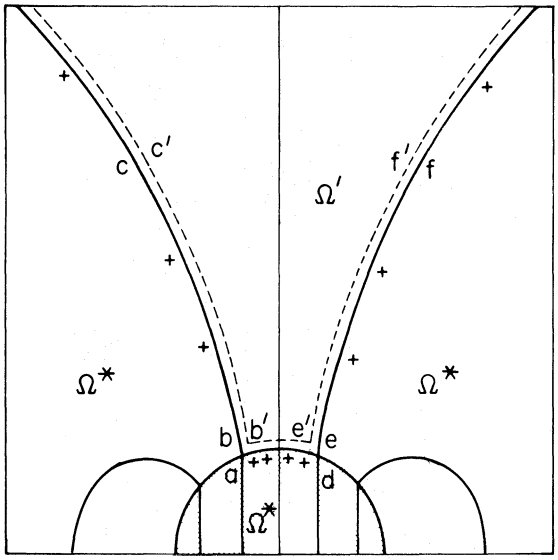

FIG. 2.—Magnetosphere of a rotating neutron star (angular velocity Ω^*) with an antiparallel dipole field and a polar gap above the surface in the polar region *ad*. There is zero charge in the magnetosphere between the solid and dashed lines; additional charge is designated only within the star. The magnetosphere between the equator and the cone of *abc* and *def* corotates with the star. The magnetosphere within the cone of $c'b'e'f'$ rotates with angular velocity $\Omega' < \Omega^*$: Ω' is constant only along magnetic field lines. Significant departures of $\boldsymbol{E}\cdot\boldsymbol{B}$ from zero occur only within the polar gap $ab'e'd$.

As h increases and approaches r_p, equation (15) begins to fail. The plasma within the polar column retreats further from the boundary *cbadef* and ultimately disappears, so that the entire column above the polar cap within r_p is empty. An analytic solution is possible for $R \gg r_p$ and a uniform magnetic field normal to the stellar surface: $\boldsymbol{E}\cdot\boldsymbol{B}$ falls off exponentially along all field lines in the gap like $\exp(-z/r_p)$; its maximum values are achieved along the central field line, and it falls to zero along the boundary field lines at r_p (cf. Appendix). But for any field structure the combination of $\oint \boldsymbol{E}\cdot d\boldsymbol{s} = 0$, $\boldsymbol{E}\cdot\boldsymbol{B} = 0$ along a gap boundary field line, and the known $\boldsymbol{E} \perp \boldsymbol{B}$ within the stellar surface gives

$$\Delta V_{\max} = \int_0^\infty \boldsymbol{E}\cdot\hat{\boldsymbol{B}} dz = \frac{\Omega B_s}{2c} r_p^2 = \frac{\Omega\Phi}{2\pi c} , \qquad (17)$$

where Φ is again the total open field line flux from the polar cap (which is sensitive only to the dipole contribution). This is, of course, just the result of equation (8) and of equation (3.7) of Sturrock (1971). Equation (17) gives the maximum possible potential drop along any magnetic field line within a polar gap—a relation which will have a direct application to predictions of pulsar turnoff when sufficiently long periods are reached (§ VII).

V. LIMITATION OF GAP HEIGHT BY VACUUM BREAKDOWN

The gap thickness h will grow at a speed near c if the outward flow of positive charge through the light cylinder approaches that of equation (10). But the potential difference across the gap grows like h^2, so that ultimately the gap will be discharged by an avalanche of electron-positron pairs. In the huge gap magnetic field any γ-ray whose energy greatly exceeds $2m_e c^2$ may generate an $e^- e^+$ pair. (Even the natural background for such γ-rays exceeds $10^5\ \mathrm{s}^{-1}$ onto the polar cap.) In the $\boldsymbol{E}\cdot\hat{\boldsymbol{B}}$ electric field within the gap, both created particles are accelerated along magnetic field lines to extreme relativistic energies comparable to $e\Delta V$ of equation (16). (For $B \approx 10^{12}$ gauss, $\Omega \approx 2\pi\ \mathrm{s}^{-1}$, and $h \sim 10^3$ cm, $e\Delta V \sim 10^{11}$ eV.) The electrons moving along the curved magnetic field lines emit "curvature radiation," the photons of which have a characteristic energy

$$E_{\mathrm{ph}} = \hbar\omega \approx \tfrac{3}{2}\gamma^3 \hbar c/\rho , \qquad (18)$$

where ρ is the radius of curvature of the field line along which the electron/positron of energy γmc^2 moves. These photons are emitted within an angle γ^{-1} of the velocity of the relativistic charge particles that radiate them. For e^- or e^+ which have been accelerated to energies $e\Delta V \gtrsim 10^{11}$ eV, these curvature radiation photons are sufficiently energetic that they may themselves produce additional electron/positron pairs on neighboring magnetic field lines. The mean

free path l of a photon of energy $\hbar\omega > 2mc^2$ moving through a region of magnetic field is (Erber 1966)

$$l = \frac{4.4}{(e^2/\hbar c)} \frac{\hbar}{mc} \frac{B_q}{B_\perp} \exp\left(\frac{4}{3\chi}\right);$$

$$\chi \equiv \frac{\hbar\omega}{2mc^2} \frac{B_\perp}{B_q} \qquad (\chi \ll 1). \tag{19}$$

Here $B_q = m^2c^3/e\hbar = 4.4 \times 10^{13}$ gauss; $B_\perp \equiv B \sin\theta$, with θ the angle between the direction of propagation for the photon and the magnetic field $\boldsymbol{B}$. (The mean free path is infinite and no pair production takes place if $B_\perp = 0$.) In a complete discharge of the gap, the charged particles produce curvature radiation that goes on to produce further pairs that are accelerated and produce more pair-producing curvature radiation, until a pair avalanche is formed (fig. 3). Such a discharge will grow exponentially in time when the relevant photon mean free path l becomes comparable to the gap thickness h. We shall consider a quasi-steady discharge in which $l \approx h$: the precise value of l is not too important, since the useful condition we derive specifies χ of equation (19) and small changes in χ correspond to exponentially large changes in l. (The extreme sensitivity of the discharge growth to small variations of the gap thickness may be reflected in the erratic nature of pulsar subpulses.) Curvature radiation photons are initially made almost tangent to $\boldsymbol{B}$ so that locally $\sin\theta = B_\perp/B \approx 1/\gamma \approx 0$. To reach a

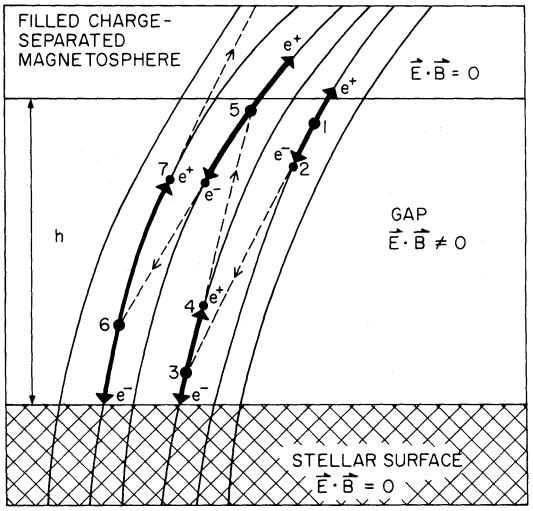

FIG. 3.—Breakdown of the polar gap. The solid lines are polar field lines of average radius of curvature ρ; for a pure dipole field $\rho \sim (Rc/\Omega)^{1/2} \sim 10^8 P^{1/2}$ cm, but for a realistic pulsar one expects $\rho \sim 10^6$ cm if many multipoles contribute near the surface. A photon (of energy $> 2\,mc^2$) produces an electron-positron at *1*. The electric field of the gap accelerates the positron out of the gap and accelerates the electron toward the stellar surface. The electron moves along a curved field line and radiates an energetic photon at *2* which goes on to produce a pair at *3* once it has a sufficient component of its momentum perpendicular to the magnetic field. This cascade of pair production—acceleration of electrons and positrons along curved field lines—curvature radiation—pair production results in a "spark" breakdown of the gap.

$B_\perp$ sufficient for a significant probability for pair production, they must go a distance directly proportional to the field line curvature ρ. After going a distance h,

$$B_\perp \sim hB/\rho\,. \tag{20}$$

From equation (19), the condition that the curvature radiation photons produce a pair in the gap is that $\chi^{-1} \approx 15$, so that

$$\frac{3}{2}\frac{\hbar c}{\rho}\left(\frac{e\Omega Bh^2}{mc^3}\right)^3 \frac{1}{2mc^2}\frac{h}{\rho}\frac{B}{B_q} \approx \frac{1}{15}, \tag{21}$$

or

$$h \approx 5 \times 10^3 \rho_6^{2/7} P^{3/7} B_{12}^{-4/7}\ \text{cm}, \tag{22}$$

where $B_{12} = \hat{r}\cdot\boldsymbol{B}_s/10^{12}$ gauss, $\rho_6 = \rho/10^6$ cm, and P is the pulsar period. In subsequent calculations we assume that the typical radius of curvature of the magnetic field lines very near the pulsar surface is $\sim 10^6$ cm. This would not be the case if the field were strictly dipolar, but it seems more reasonable to assume the field has many higher multipole components which will contribute most strongly near the surface; in any case h is only weakly dependent on ρ. We emphasize that the fundamental criterion for determining the gap parameters, $\chi^{-1} \approx 15$, has very little latitude so that curvature photon energies do not depend sensitively upon other, unknown, parameters:

$$E_{\rm ph} \approx \gamma^3\hbar c/\rho \propto \Omega^3 B^3 h^6 \rho^{-1} \propto (\rho^5\Omega^3 B^{-3})^{1/7}\,.$$

The potential difference across the gap for $B_s = 10^{12}$ gauss, $\Omega = 2\pi$, and $\rho = 10^6$ cm is

$$\Delta V \approx \frac{\Omega B_s h^2}{c} = 1.6 \times 10^{12} B_{12}^{-1/7} P^{-1/7} \rho_6^{4/7}\ \text{V}, \tag{23}$$

so that electrons and positrons in the gap may be accelerated to relativistic energies with $\gamma \sim 3 \times 10^6$. The component of the electric field along $\boldsymbol{B}$ in the gap is

$$E \simeq 2\frac{\Omega B_s}{c}(h - z), \tag{24}$$

which vanishes at the top $z = h$. At the bottom, $z = 0$, with $h \sim 5 \times 10^3$ cm, $P = 1$ s, the electric field is of order 10^9 V cm^{-1} at breakdown, entirely negligible relative to that needed to pull ions from the surface.

It remains to be shown that the curvature radiation from the particles produced and accelerated in the gap can lead to a quasi-steady discharge of the gap once h grows to the value determined by equation (22). We have considered the energies achieved by particles accelerated in the gap, the typical photon energies of the curvature radiation, and the mean free path of these photons: it is not guaranteed that an "interesting" number of photons is produced per charged particle as it traverses the gap. The rate of energy loss

through curvature radiation by an electron or positron of energy γmc^2 is

$$P = \frac{2}{3}\frac{e^2}{c^3}\gamma^4\left(\frac{c^2}{\rho}\right)^2 . \tag{25a}$$

Thus, in traveling a distance of order h the number of photons of characteristic energy $1.5\gamma^3\hbar c\rho^{-1}$ radiated by the electron or positron is

$$N_{\rm ph} \approx \frac{4}{9}\frac{e^2}{\hbar c}\frac{h}{\rho}\gamma mc^2 \approx 50 \tag{25b}$$

for the parameters of a typical pulsar. (Since the spectrum of curvature radiation goes like $\omega^{1/3}$ for $\omega \lesssim 1.5\gamma^3 c\rho^{-1}$, many more lower-energy photons are emitted.) This number of photons per particle would seem to be adequate for maintaining a discharge in a quasi-steady state. Two-stream instabilities and electron interactions with photons from the discharge-heated polar cap will be considered elsewhere. The former is unimportant for the extreme relativistic plasma of the gap. The latter is significant only for a very fast pulsar such as that in the Crab. (We note that a pair avalanche discharge of the gap will not be sustained by pair production just below the stellar surface even if positrons formed there escape into the gap. Curvature radiation, or synchrotron radiation, from such positrons may have sufficient energy to produce additional pairs in the stellar surface, but it is always directed away from that region. Pair production within the gap seems crucial.)

In all except the slowest pulsars, the potential drop across the gap of equation (23) is much less than the maximum possible, ΔV of equation (8). Therefore, most of the pulsar energy loss given in equation (11) is not used in gap acceleration. We note that this is one main cause for the differences between many of our results and those of Sturrock (1971). The upper bound for the energy flux carried by relativistic positrons into the magnetosphere above the gap ($\dot{E}_+$) is

$$\dot{E}_+ \approx \Delta V \rho_e c\pi r_p^2 = \Delta V \frac{\Omega}{2\pi}\Phi$$

$$\approx 10^{30} B_{12}^{6/7}\rho_6^{4/7}P^{-15/7}\ \text{ergs s}^{-1} , \tag{26}$$

where P is in seconds. We shall show in § VIII that a substantial fraction of this energy flux is expected to be converted to coherent microwave radiation in the near magnetosphere above the gap. Thus, equation (26) also represents an upper bound to the pulsar radio luminosity. This result is not inconsistent with the radio luminosities of those pulsars to which distances can be estimated (see, e.g., Cavallo 1972; Prentice and ter Haar 1969).

The flow of energetic electrons back onto the polar cap will heat it. If we make the extreme assumptions that all of the cap is irradiated all of the time with the maximum breakdown electron energy flux, and that inward heat conduction away from the surface is negligible, then in equilibrium the energy flux radiated away from the surface is

$$\mathscr{F} = \tfrac{1}{2}\Delta V \rho_e c$$

$$\approx 2 \times 10^{21}\ \text{ergs cm}^{-2}\,\text{s}^{-1} \tag{27}$$

for a typical $P = 1$ s pulsar. This flux, for all radio pulsars, is about an order of magnitude less than that needed to heat the surface to sustain a temperature T ($\geq T_c$) such that the ion flux could discharge the gap. But, even if it were sufficient, the e^--e^+ discharge would be a necessary prerequisite for maintaining the surface temperature. Therefore in either circumstance the gap must grow to a size sufficient for the electron-positron discharge to be maintained. In the case of the Crab pulsar the energy flux of the returning electrons is quite sufficient to lead to the thermal emission of ions; thus the present model is not directly applicable. We will consider the Crab pulsar in a separate paper.

VI. SPARKS

a) Structure and Drifting of Sparks: Observational Consequences

When a discharge begins at some point on the polar cap, the $\boldsymbol{E}\cdot\hat{\boldsymbol{B}}$ that has built up across the gap rapidly falls there. This would be expected to inhibit the formation of another simultaneous discharge within a distance $\sim h$. Thus the gap discharges through a group of localized "sparks." These sparks inject energetic positron beams into the magnetosphere beyond the gap. In a manner to be discussed in § VIII, these positrons ultimately produce the plasma and the bunching which results in the conversion of much of their energy into coherent microwave radiation. But regardless of the relevance of a particular detailed radiation mechanism, it is reasonable to suppose that the location of the sparks on a polar cap determines the geometrical pattern of instantaneous subpulses within a pulsar's integrated pulse profile. The intensity of the spark discharge may fluctuate as the electron-positron plasma increases (decreases) and the potential drop decreases (increases), but presumably it only rarely turns off entirely. Within the polar gap, sparks circulate in a calculable way with periods which seem to match those of the observed so-called drifting subpulses. Electrons and positrons in a spark do not exactly corotate with the stellar surface until $\boldsymbol{E}\cdot\boldsymbol{B} = 0$ everywhere along it. (This drift relative to the surface would appear as a displacement rather than a subpulse motion if the discharged particles always moved away from a fixed point on the polar cap of the star; it is only the flow back to the surface that causes the spark region to drift.)

We consider a spinning neutron star whose magnetic polar cap is not aligned with its spin axis—the sort of geometry which would give possible pulsar-like radiation patterns if beams of radiation are associated with the outflowing positrons beams. For simplicity we approximate the magnetic field within the polar gap as constant in magnitude and normal to

the stellar surface there. Then in the absence of the gap when corotation prevailed the electric field was tangent to the surface and had a magnitude $|[(\boldsymbol{\Omega} \times \boldsymbol{r})/c] \times \boldsymbol{B}|$. The presence of the gap changes the tangential velocity within the gap and thus alters the corotation velocity given by

$$\boldsymbol{v} = \frac{\boldsymbol{E} \times \boldsymbol{B}}{B^2} c \,. \tag{28}$$

In figure 4, a spark is represented in a polar gap "pillbox" as it passes over the horizon. In the near-field zone

$$\oint \boldsymbol{E} \cdot d\boldsymbol{s} = 0 \,, \tag{29}$$

an exact result when the magnetic field has axial symmetry about the spin axis. Therefore,

$$\oint \Delta \boldsymbol{E} \cdot d\boldsymbol{s} = 0 \,,$$

where $\Delta \boldsymbol{E}$ is the change in electric field caused by the gap. For the closed contour *abfea* of figure 4, $\Delta \boldsymbol{E} = 0$ on the segment *ab* along $\boldsymbol{B}$ because $\boldsymbol{E} \cdot \boldsymbol{B} = 0$ at the polar gap boundary. Similarly $\Delta \boldsymbol{E} = 0$ on *bf* which lies just within the stellar surface where equation (2) is always satisfied. Therefore,

$$\int_a^e \Delta \boldsymbol{E} \cdot d\boldsymbol{s} = \int_f^e \boldsymbol{E} \cdot \hat{\boldsymbol{B}} ds \,. \tag{30}$$

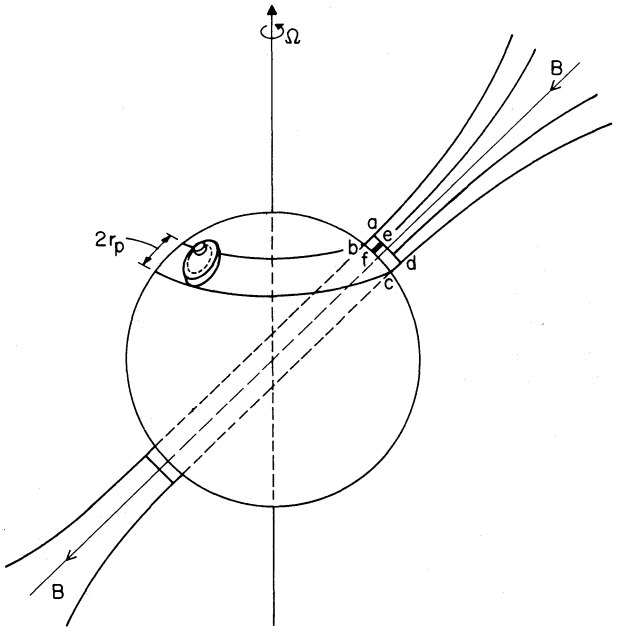

FIG. 4.—Schematic of a rotating neutron star with dipole moment somewhat inclined to the rotation axis. The polar cap, of base diameter $2r_p$, moves at fixed latitude. A spark *ef* in the gap *abcd* drifts counterclockwise on a circular path (*dashed line*) on the polar cap centered on the magnetic field axis. This spark feeds relativistic particles onto field lines: coherent microwave radiation is produced tangentially to these field lines far above ($\sim 10^8$ cm) the stellar surface.

For the right-hand side of equation (30), the potential drop over the length of a spark, we can use ΔV for breakdown given by equations (23) and (22). But $e\Delta V$ is $\sim 10^{12}$ eV for all pulsars, depending only upon B and P to the 1/7 power. With the approximation $\langle ae \rangle \sim r_{p_+}/2$, the average drift velocity of the sparks around the magnetic pole of the neutron star has a magnitude

$$\Delta v = \frac{\Delta V}{B_s r_{p_+}} c \,. \tag{31}$$

The time ($\hat{P}_3$) for a spark to make a complete precession revolution about the magnetic pole is given by

$$\hat{P}_3 = 2\pi \frac{B r_{p_+}{}^2}{\Delta V c} \,. \tag{32}$$

Then from equations (4), (6), and (32)

$$\frac{\hat{P}_3}{P} \approx \frac{2\Phi_+}{\Delta V c} \approx 5.6 \frac{B_{12}}{P^2} \text{ s} \tag{33}$$

with the period P of equation (33) in seconds, $R = 10^6$ cm, and $e\Delta V = 10^{12}$ eV. An arbitrary observer's direction relative to a pulsar beam will generally permit him to see radiation from sections of the full beam; $\hat{P}_3$ will be the period for a subpulse which will appear to drift through the beam envelope, and disappear to return to its initial position. The sense of the observed drifting depends on whether the direction to the observer is above or below (relative to the rotation axis) the magnetic dipole axis. Equation (33) can be compared with the reported periodicity P_3 for drifting subpulses. (A similar drifting of the spark discharge might be expected in the Sturrock 1971 model; however, the potential drop in his model is essentially that given in our eqs. [8] and [17] and leads to $\hat{P}_3 \approx P$ for all pulsars.)

A schematic representation of typical drifting subpulses is given in figure 5. A long-time average over many pulses gives a broad envelope whose width is typically of order 5–10 percent of the pulsar period. But a single pulse consists of much narrower subpulses which appear to move through the pulse envelope and disappear. The period P_3 is that for a particular subpulse distribution recurring. The period P_2 is the separation between successive subpulses. (A more complete discussion of the kinds of rapid fluctuations in intensity and phase characteristic of many pulsars is given by Taylor and Huguenin 1971.) The spark model very strongly suggests the association of P_3 with the period $\hat{P}_3$ for drifting sparks; i.e.,

$$P_3 \approx \hat{P}_3/n \,, \tag{34}$$

where n is the total number of spark discharges around a polar cap. Backer (1973) summarizes the observations of P_3 with the categorization $P_3 \leq 10P$ for $P > 0.75$ s and $P_3 \geq 10P$ for $P < 0.75$ s. Remarkably, this is just the separation given by equation (33) with $B_{12}/n = 1$. Of course, magnetic field irregularities can

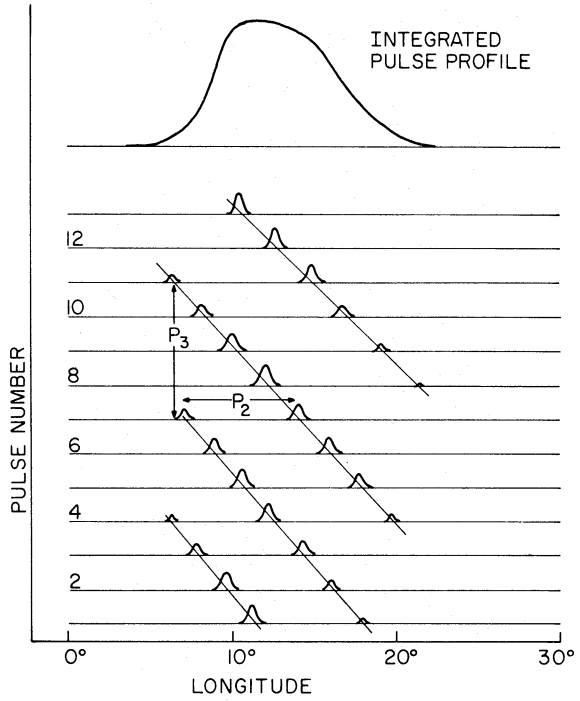

FIG. 5.—Schematic (after Backer 1973) of integrated pulse profile, arrival times of individual pulses, and definition of P_2, P_3 for those pulsars showing the "drifting subpulse" phenomenon. Arrival times of individual pulses are given in terms of a longitude for which 360° corresponds to the full pulsar period.

make the drifting more complicated and may even, in many pulsars, pin sparks and prevent "drifting." But the agreement with the predicted P_3 is nontrivial since, except for B_{12}, there is no sensitivity to unknown parameters, and there is abundant independent support for about this magnetic field strength.

The "period" P_2 has a natural interpretation in terms of the distance between sparks. If we assume (cf. § VIII) that the spark-injected positrons somehow cause coherent radiation of a subpulse to be emitted far from the polar gap tangent to the open field line along which they move, then there is a predicted relationship between P_2, P, the total measured width of the long-time-averaged pulse envelope (θ_w), and the spacing (s) between sparks on the star's polar cap. In the dipole-dominated region at a fixed distance from the star the angle θ between the tangent to an open field line and the polar axis, and the distance from the

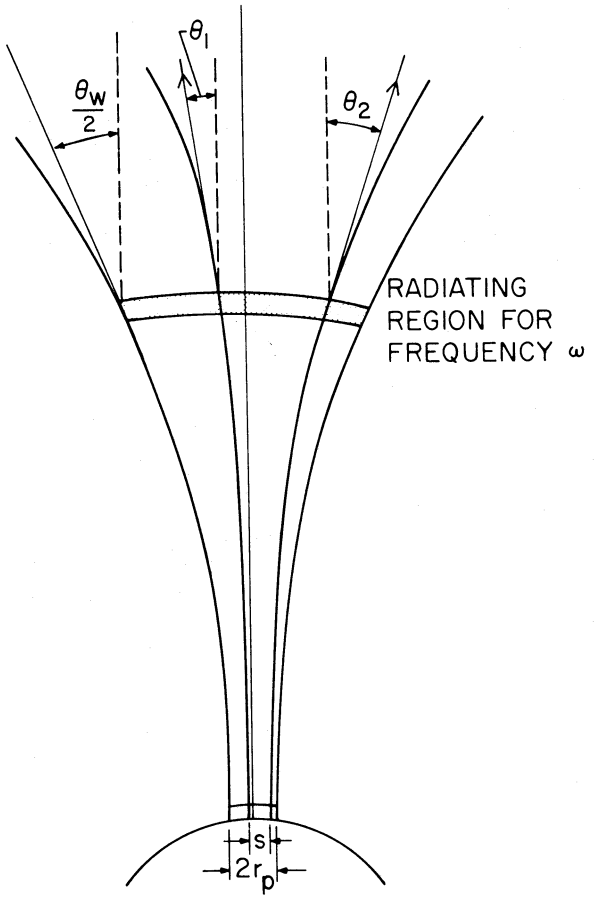

FIG. 6.—Notation for emission angles of radiation initiated by sparks, a distance s apart and from sparks at the limits of the polar cap, $2r_p$ apart. $2\pi P_2 P^{-1} \sim \theta_1 + \theta_2$.

pole on the polar cap r_{p_+} are related by $\theta \propto r_{p_+}$ (see fig. 6). Then

$$\left(\frac{s}{r_{p_+}}\right) \sim \frac{P_2}{P}\left(\frac{360°}{\theta_w}\right). \tag{35}$$

Backer lists P_2 for three "linearly" drifting pulsars for which the period can be obtained without ambiguity. These are compared in table 1 with calculated P_2. In equation (35), for P_2, s is expected to lie not far from the gap height h (in the limit $h \ll r_{p_+}$); for $s = h$ we obtain the results of table 1. The agreement between

TABLE 1

COMPARISON OF OBSERVED AND CALCULATED* SUBPERIODS P_2 FOR THREE PULSARS

Pulsar	P(s)	θ_w(°)	P_2(theory) (ms)	P_2(obs.) (ms)
2303 + 30.....	1.6	8	20	20
2016 + 28.....	0.6	12	10	11
0809 + 74.....	1.3	30	50	60

* From eq. (35).

theory and observation does not discourage the interpretation of P_2 as an expected spark separation phenomenon.

With this view of pulsar radiation maintained by a distribution of sparks across the polar gap, one is tempted to look for analogies with the observed behavior of more familiar spark discharges. Abrupt changes in spark patterns may correspond to sudden changes in pulse structure observed for some pulsars (e.g., PSR 1237+25, discussed by Taylor and Huguenin 1971).

b) Time Structure of Sparks

When part of a polar gap begins to break down into a spark, the initial electrons and positrons feel the full potential ΔV of equation (23) ($\sim 10^{12}$ V). This potential does not drop greatly until the electron and positron density reaches that of equation (1) as it is created and pulled apart in the gap electric field, equation (24). Only then does the net charge density in the gap approach that necessary to bring $\boldsymbol{E}\cdot\boldsymbol{B}$ back to near zero. The time (τ_0) needed for the conversion of a photon to an e^--e^+ pair in the gap is $\sim l/c \sim h/c$. To reach the density of equation (1), 10^{15} pairs cm^{-2} must be created. Although the precise cross-sectional area of a spark is unknown, the growth and fluctuation time scales should be $\sim(30\text{–}40)\tau_0 \sim 10\mu$s, and a similar time scale would be expected in spikes in very short-time-resolution observations of individual pulses in pulsars. Spikes with this kind of width have indeed been reported by Hankins (1971).

A quantitative description of the time dependence of the energy and flux of spark positrons injected into the region above the gap would be needed to support a more exact calculation of the coherent radiation they ultimately produce than that which we shall offer in § VIII. Roughly during the beginning of the growth time τ the injected positrons have $\gamma_+ \sim 3 \times 10^6$. This will drop toward $\gamma \sim 1$ as the separating gap plasma reaches the density ρ_e. However, even a drop of about 2 in γ_+ will stop the curvature radiation from producing additional pairs in the gap. The characteristic drop in γ_+ from its maximum at the beginning of the pulse to much smaller values as J_+ grows is an important feature of spark-injected positrons for their subsequent role in causing coherent microwave radiation.

VII. PULSAR TURNOFF; APPARENT AGING EFFECTS

As pulsar periods lengthen, the gap thickness h grows in order to keep $e\Delta V \approx 10^{12}$ eV and maintain spark discharges. But for sufficiently large h (comparable to r_{p_+}), ΔV no longer continues to increase significantly with h. Instead, the limit of equation (17) is approached. When this limit falls below the potential drop necessary for forming any spark, current from the polar cap is terminated and the spinning neutron star is no longer a pulsar. This is essentially the pulsar turnoff mechanism proposed by Sturrock (1971).

When the gap thickness h approaches and exceeds r_{p_+}, as it ultimately must when the pulsar period P continually increases, the gap electric field begins to drop exponentially with height z: $E \approx \exp(-z/r_p)$. Then even as $h \to \infty$, the pair-produced discharge electrons produce curvature radiation to continue the discharge development only within r_{p_+} of the pulsar's surface. Thus in a discharge the largest effective distance an electron-produced γ-ray propagates before it should make a pair is $\sim r_{p_+}$ when it is moving through a perpendicular magnetic field

$$B_\perp \approx (r_{p_+}/\rho)B\,, \tag{36}$$

where ρ is the radius of curvature of the flux line along which the electron was accelerated. This is the analog of equation (20) for gaps with $h \to \infty$. The maximum energy of such an electron is given by equation (17):

$$e\Delta V_{\max} = \frac{1}{2}\frac{\Omega B_s}{c} r_{p_+}{}^2 = \frac{\Omega\Phi_+}{2\pi c}\,, \tag{37}$$

where r_{p_+} is given by equation (4). As in § V, the maximum electron energy results in the characteristic curvature radiation whose energy is given in equation (18). For pair creation to continue, the combination defined in equation (19) is

$$\chi \equiv \frac{\hbar\omega}{2mc^2}\frac{B_\perp e\hbar}{m^2c^3} \gtrsim \frac{1}{15} \tag{38}$$

(cf. eq. [21]). From the inequality (38) and equations (37), (4), (36), and (18), the maximum period $P_{\rm crit}$ above which a gap discharge cannot exponentiate is

$$P_{\rm crit} = 1.7 B_{12}{}^{8/13} R_6{}^{21/13} \rho_6{}^{-4/13} (15\chi)^{-2/3}\ \text{s}\,. \tag{39}$$

This reduces to essentially the result of Sturrock (1971) if pure dipole curvature is used for ρ_6. This equation is not of immediate use in analyzing observed pulsars without some independent way of determining the magnetic field strength. The canonical way to determine $B_s{}^d$ is through equation (11), inverted for B:

$$B^2 = \frac{Ic^3}{(2\pi)^2 R^6} P\dot{P}\,, \tag{40}$$

where I is the total moment of inertia of the neutron star. The parameter I/R^6 varies by almost two orders of magnitude for the full range of stable neutron stars (see, for example, Baym *et al.* 1971). However, theoretical models for the genesis of neutron stars suggest that they should be formed with a mass near the Chandrasekhar limit $\sim 1.3\ M_\odot$ (see Ruderman 1972*a*); in that case I/R^6 has a much more limited range. In the results discussed below we adopt the $M = 1.25\ M_\odot$ neutron star model of Baym *et al.* (1971) with $I = 6.24 \times 10^{44}$ g cm^2, $R = 8.1$ km. In figure 7 we have plotted $P\dot{P}$ versus the pulsar "age" $P/\dot{P}$ for the 28 pulsars for which P and $\dot{P}$ are known (we have not included the data for the Crab and Vela pulsars): the data are taken from the compilation of Terzian (1973). Equations (39) and (40) together with the inequality $P \le P_c$ and $\rho_6 = 1 = 15\chi$ imply that ob-

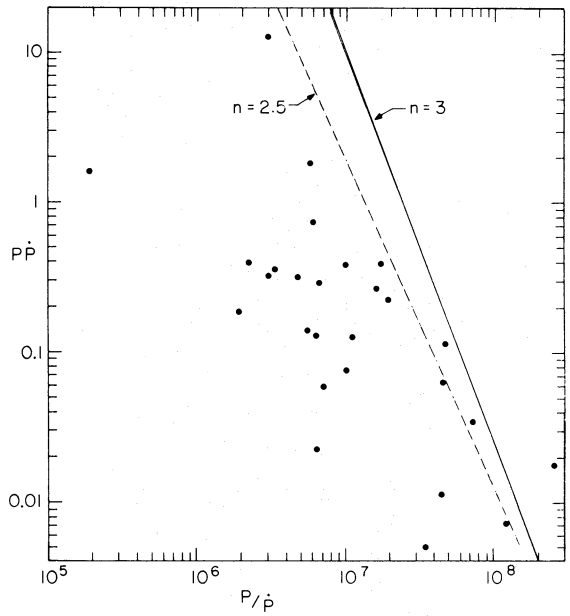

FIG. 7.—Relation between $P\dot{P}$ [assumed proportional to $(B_s^d)^2$] and the pulsar "age" $\equiv P/\dot{P}$. The data is taken from Terzian 1973. For $P\dot{P}$, P is measured in seconds and $\dot{P}$ in nanoseconds per day while $P/\dot{P}$ is measured in years. The solid line is the theoretical pulsar turnoff boundary given by eq. (41). The dashed line assumes the pulsar "braking index" $n = 2.5$ as in the Crab pulsar rather than $n = 3$ as in eq. (11). Note that the relatively young pulsar with the largest $P\dot{P}$, PSR 0525+21, has the longest period (yet observed) and presumably the strongest dipole field.

servable pulsars should lie to the left of the line shown as

$$P\dot{P} = \text{const.}\ (P/\dot{P})^{-13/5}\ . \qquad (41)$$

It has no arbitrary parameters once the mass $M = 1.25\ M_\odot$ is chosen. For less massive neutron stars, I/R^6 is smaller and this critical boundary line moves further to the left.

For the parameters chosen, all pulsars but one do indeed lie to the left, although the slope of $-13/5$ seems to be somewhat steep for the data. This slope is of course changed if the $-\dot{\Omega} \propto \Omega^3$ braking relationship which resulted from equation (11) is replaced by one with an arbitrary braking index n: $-\dot{\Omega} \propto \Omega^n$. Since there are other contributions to the braking torque acting on the neutron star in addition to that due to the completion of the homopolar generator circuit in the neutron star (for example, the low-frequency radiation torque in the oblique rotator case), the measurable braking index n is not known theoretically, even if the total current through the polar caps of the pulsar were determined. The only pulsar for which n has been measured is the Crab pulsar (for which the present pulsar model is not directly relevant). Boynton *et al.* (1972) report $n = 2.5$. This seems to give a better boundary for the observed points of figure 7 than does $n = 3$, although the absence of a theoretical model introduces an arbitrary proportionality constant into equation (41). Although the slope of the critical $P\dot{P} \sim B^2$ versus age cutoff curve is uncertain, the existence of some such line with the approximate slope shown follows in the present pulsar model from equation (36). It implies certain points in the interpretation of a plot of $P\dot{P}$ versus $P/\dot{P}$: (i) The older pulsars, defined as having greater "ages" $(P/\dot{P})$, are observable as pulsars only for smaller $P\dot{P} \sim B^2$. Because $P/\dot{P}$ specifies how long a pulsar lives at that age, a bunching of pulsars is expected near the critical turnoff boundary with a preponderance of older pulsars with smaller $P\dot{P}$ since these have the largest $P/\dot{P}$. This will, of course, appear as a decrease in $P\dot{P} \sim B^2$ with age in old pulsars if all observed points are interpreted (incorrectly) as corresponding to a single approximate evolutionary track (Gunn and Ostriker 1970). (ii) Very long-period pulsars, to be observable, have particularly large surface magnetic fields. (Indeed, the longest period pulsar, PSR 0525+21, with $P = 3.75$ s, has the largest $P\dot{P}$ of the pulsars plotted in fig. 7.) (iii) The previous two points lead to selection effects in pulsar data and the determination of the braking index from a plot of, say, $I\Omega\dot{\Omega}$ versus $P/\dot{P}$. For a given (older) age, pulsars with high $P\dot{P}$ are missing; for a given longer period P, the smaller $B \sim (P\dot{P})^{1/2}$ are not observable as pulsars. Because of these selection effects in pulsar data, even if each pulsar had the same braking index, $n = 3$, a plot of $I\Omega\dot{\Omega}$ versus P for all pulsars would be best fitted with an index $n > 3$. Thus the fit which yielded $n = 3.4$ for this index (Ruderman 1972*a*) may not at all, as suggested, imply $n > 3$ for individual pulsars.

The contribution of the homopolar generator part of the pulsar braking torque would be expected to decrease below that of equation (11) with increasing P as spark separation increased. This would tend to make $n > 3$. A decrease in angle between $\boldsymbol{\Omega}$ and $\boldsymbol{B}$ would tend to increase gap currents and give $n < 3$ for the related part of the braking index.

VIII. COHERENT MICROWAVE RADIATION FROM THE NEAR MAGNETOSPHERE

In the continuing breakdown of the polar gap discussed in § V, the primary positrons accelerated through the gap and into the magnetosphere give most of their curvature radiation after they have passed above the gap. The maximum energy of these positrons after crossing the gap is (see eq. [23])

$$E_{\max} = \gamma_{\max} mc^2 = \frac{e\Omega B h^2}{c}$$

or

$$\gamma_{\max} = 1.2 \times 10^7 \frac{B_{12} h_4^{\,2}}{P}\ . \qquad (42)$$

Once above the gap, they are in a region where $\boldsymbol{E}\cdot\boldsymbol{B} = 0$, and further acceleration ceases in the near magnetosphere. These positrons move along curved magnetic field lines whose radius of curvature near the stellar surface, ρ, is assumed to be of the same order

as the stellar radius since many multipolar components probably contribute to the near magnetic field. The curvature radiation produced by the positrons has a characteristic photon energy

$$\hbar\omega_c = \frac{3}{2}\gamma_{\max}{}^3\frac{\hbar c}{\rho} = 5.4 \times 10^4 \frac{B_{12}{}^3 h_4{}^6}{\rho_6 P^3}(2mc^2)\,. \quad (43)$$

(The spectrum of curvature radiation has a maximum at $\omega_c = \frac{3}{2}\gamma^3 c/\rho$ above which the spectrum falls exponentially and below which the intensity $\sim\omega^{1/3}$.) As emphasized in the discussion following equation (22), because of the nature of the breakdown condition, the photon energy of equation (43) is not a very sensitive function of the various parameters. With the parameters of § V, i.e., $B_{12} = 1$, $\rho_6 = 1$, $P = 1$ s, and h_4 determined to be 0.5, we have $\hbar\omega_c \approx 800$ MeV. The lifetime of the primary positrons against radiating away their energy by transverse (curvature) radiation is

$$\tau = \frac{E}{\dot{P}} = \frac{\gamma mc^2}{\frac{2}{3}(e^2/c^3)\gamma^4(c^2/\rho)^2}\,. \quad (44)$$

The most energetic positrons, those with $\gamma \approx \gamma_{\max}$, radiate away their energy in a distance $c\tau \approx 10^6$ cm above the polar cap if $\rho \approx 10^6$ cm while less energetic positrons produced in the latter phases of a discharge keep most of their energy out to much greater distances since $c\tau \propto \gamma^{-3}$. It might appear that the distance through which the most energetic positrons travel before radiating away much of their energy is a sensitive function of their assumed total energy. But this is not really the case because it is these same positrons and their curvature radiation that must also produce the gap breakdown. Were $\gamma_{\max}$ small enough that the distance for conversion of positron kinetic energy to curvature radiation greatly exceeded 10^6 cm, the gap would not break down. Rather it would grow higher to accelerate subsequent positrons to greater energies. Thus the most energetic positrons must always radiate away most of their energy within $\sim 10^6$ cm of the stellar surface. As the spark discharge develops and fluctuates, somewhat less energetic positrons are produced. Most may reach the region sufficiently far above the stellar surface where ρ increases enough to allow them to leave the near magnetosphere without much more radiative loss.

The curvature radiation photons produced by the primary positrons have energies well in excess of $2mc^2$. They originate sufficiently close to the neutron star (within 10^6 cm for the most part) that their mean free path for pair production on magnetic field lines is again $\sim 10^4$ cm. Thus most of the energy in the more energetic positrons ($\gamma \approx \gamma_{\max}$) is converted, through this two-step process, to outward-moving electron-positron pairs in the near magnetosphere. Since these pairs are produced in the magnetosphere in which $\boldsymbol{E}\cdot\boldsymbol{B} = 0$, there is no acceleration along the field lines. Further curvature radiation by these pairs has a characteristic frequency

$$\omega_c = \frac{3}{2}\gamma_{\pm}{}^3\frac{c}{\rho}\,. \quad (45)$$

If initial transverse and relative energies of the photon-produced e^--e^+ pair are neglected, then $\gamma_\pm$ is simply $\hbar\omega_c/2mc^2$ as given in equation (43). We shall make this approximation in all further estimates. But this neglect, which assumes that there exists a comoving frame in which all e^- and e^+ are at rest, is probably at best crude and may be quite poor. At distances much more than 10^6 cm above the stellar surface where the field lines are mainly dipolar, the radius of curvature of the open field lines at r is

$$\rho \geqslant 2\left(\frac{rc}{\Omega}\right)^{1/2} = 1.4 \times 10^9 (r_8 P)^{1/2}\ \text{cm}\,; \quad (46)$$

the equality holds for the last open field lines (those with "feet" at the edge of the polar cap). With $\gamma_\pm \approx 800$, the frequency of equation (45) falls into the radio band ($\omega_c/2\pi \approx 10^9$ Hz) for $\rho \approx 10^9$ cm.

However, the efficiency for single-particle, incoherent, curvature radiation in the magnetosphere is negligible. The fraction f of the total energy E radiated by a particle as it moves along a trajectory of curvature ρ is, from equations (43) and (44):

$$f = \frac{P\rho/c}{E} = \frac{2}{3}\frac{e^2}{\hbar c}\frac{\hbar\omega_c}{mc^2}\,, \quad (47)$$

where $\hbar\omega_c$ is the photon energy of the curvature radiation. Since $\omega_c \sim 10^{10}\ \text{s}^{-1}$, $f \approx 10^{-13}$. That single-particle incoherent radiation is inadequate in explaining pulsar radiation is, of course, well known and not very surprising—the remarkably high brightness temperatures of order 10^{30} °K of some pulsar radio emission certainly means that the radiation must be produced coherently. However, the stream of secondary electron-positron pairs produced in the near magnetosphere is ultimately bunched at about that distance from the neutron star at which f_{cr} is in the radio band, where f_{cr} is the frequency of curvature radiation into which the pair kinetic energy is most efficiently pumped by the bunching. This bunching of the relativistic pair plasma stream ($\gamma_\pm \approx 800$) arises from its collective Coulomb interaction with an even more relativistic stream of positrons which passes through it. These are the primary positrons with initial $\gamma \approx \gamma_{\max}$ after γ has been reduced through curvature radiation and also those gap-produced positrons produced when the fluctuating potential drop falls below that of equation (16). Because of their reduced γ's, these positrons have negligible further energy loss, and they catch up with and ultimately pass through the slower moving pairs. This beam of positrons pumps the classical "two-stream instability" that leads to the bunching that enormously enhances coherent curvature radiation from the pair plasma as discussed below. Bludman, Watson, and Rosenbluth (1960) have

shown that in the *rest frame* of a cold neutral plasma through which a low-density relativistic charged beam moves, there is a most rapidly growing plasma bunching instability with strong beam-plasma coupling very near the plasma frequency

$$\omega_p' \approx \left(\frac{4\pi n' e^2}{m}\right)^{1/2}, \tag{48}$$

where n' is the number density of charges in the rest frame. The wave vector of the plasma instability is directed along the relative streaming velocity, parallel to the magnetic field. In our case where this velocity is relativistic, the wavenumber of the unstable mode is $k' = \omega_p'/c$. Thus the unstable plasma wave has just the transformation properties of a photon: in an observer's reference frame in which the cold plasma itself is moving relativistically with Lorentz factor $\gamma_\pm$, this growing unstable mode has a frequency

$$\omega_p = 2\gamma_\pm \omega_p' \tag{49}$$

and $k = \omega_p/c$. Thus it has just the frequency-wavenumber relation and speed of a photon. In the plasma streams above the polar gap of the pulsar, the cold plasma is simply the stream of secondary electron-positron pairs, and the much lower-density relativistic beam which passes through it to feed the plasma instability is composed of the "primary" positrons with $\gamma < \gamma_{\max}$. The density of pairs in the plasma stream in its rest frame is $n' = n/\gamma_\pm$, where n is the pair density in the observer's frame. Because the pair plasma moves out along diverging field lines, its density decreases with increasing r. Well beyond the gap where other magnetic multipoles are unimportant the region of open, dipolar field lines gives $n \sim r^{-3}$. The maximum density of primary positrons in the gap is

$$n_{\text{primary}} \approx \Omega B_s^{(d)}/2\pi ec\,. \tag{50}$$

For $\gamma \approx \gamma_{\max}$ they produce $\gamma_{\max}(2\gamma_\pm)^{-1}$ secondary pairs above the gap. Since both the primary and secondary particles are constrained to move along the magnetic field lines, the maximum density of secondary plasma pairs in the near magnetosphere then is

$$n_{\text{secondary}} \approx \frac{\gamma_{\max}}{2\gamma_\pm}\frac{\Omega B_s^{(d)}}{2\pi ec}\left(\frac{R}{r}\right)^3. \tag{51}$$

From equations (48), (49), and (51) we calculate the frequency of the bunching mode in the observer's frame:

$$\omega_p = 2\left(\frac{2\gamma_{\max} e\Omega B R^3}{mcr^3}\right)^{1/2}. \tag{52}$$

If the frequency ω_p of equation (52) is much greater than ω_c of equation (45), then the bunching from the growing plasma wave is ineffective in enhancing the curvature radiation. Its spatial and temporal oscillations are so much more rapid than those of the emitted electromagnetic waves that effective bunching averages to zero over relevant times or distances. But as soon as ω_p drops below ω_c, the bunching can be extraordinarily effective. Because curvature radiation does not fall sharply for $\omega < \omega_c$, there is always some mode of the curvature radiation that is greatly enhanced by bunching on a time scale ω_p^{-1}. The intensity of the resulting coherent radiation depends on the bunching amplitude and on the time this mode can remain before dissipating its energy into other degrees of freedom of the plasma.

Before proceeding further with a discussion of the geometry of the radiating region and the spectrum and polarization of the radiation, we show that the bunching instability in the pair plasma that produces the coherent radiation develops sufficiently quickly and that the amount of bunching is enough to make the radiation efficient. The maximum growth rate of a bunching instability induced in a cold neutral plasma by a relativistic beam is (see Bludman *et al.* 1960)

$$(\tau')^{-1} = 0.69(\omega_b'^2\omega_\pm')^{1/3}, \tag{53a}$$

where

$$\omega_\pm' = \left(\frac{4\pi n_\pm' e^2}{m}\right)^{1/2}, \tag{53b}$$

$$\omega_b' = \left(\frac{4\pi n_b' e^2}{\gamma_b'^3 m}\right)^{1/2}. \tag{53c}$$

Equations (53a)–(53c) are valid in the rest frame of the cold plasma where $n_\pm'$, n_b' are respectively the number densities of charged particles in the plasma and in the beam. For $\gamma_\pm \ll \gamma_b \lesssim \gamma_{\max}$ we have

$$n_\pm' = \frac{1}{\gamma_\pm} n_{\text{secondary}}, \tag{54a}$$

$$\gamma_b' = \frac{1}{2\gamma_\pm}\gamma_b, \tag{54b}$$

$$n_b' = \frac{1}{2\gamma_\pm} n_b. \tag{54c}$$

Because of the diverging dipolar field lines which guide the plasma streams, both n_b and $n_{\text{secondary}}$ decrease as $(r/R)^{-3}$. If, as expected, $n_b(r \approx R) \sim n_{\text{primary}} \approx \Omega B(2\pi ec)^{-1}$, then in the observer's frame equations (51) and (53) give

$$\tau^{-1} = (\gamma_\pm \tau')^{-1} \approx \left(\frac{2e\Omega B}{mc}\right)^{1/2}\left(\frac{R}{r}\right)^{3/2}\frac{1}{\gamma_b}\left(\frac{\gamma_{\max}}{\gamma_\pm}\right)^{1/6}$$

$$\approx 60 \times \left(\frac{10^6}{\gamma_b}\right) \times \left(\frac{10^8}{r}\right)^{3/2} \text{s}^{-1} \tag{55}$$

for a $P = 1$ s pulsar. The primary positrons that survive beyond $r_{\min} \sim 10^8$ cm, where $\omega_c \sim \omega_p$, have $\gamma_b \lesssim 10^6$. There $\tau \sim 10^{-2}$ s, sufficient to put most of the relative two-stream energy into bunching within a distance of a few $r_{\min}$. The amount of bunching which can result follows from the energy put into this plasma mode: Let Z be the net charge within a bunch (due

either to excess electrons or positrons) whose characteristic dimension is

$$l \sim 2\pi c/\omega_p' . \tag{56}$$

The maximum value that Z can attain is therefore determined by an energy balance between the energy needed for bunching and that generated by the two-stream instability, E_k per pair plasma particle:

$$ZE_k \sim (Ze)^2/l . \tag{57}$$

For $\gamma_b \sim 10^6$ and $n_b \sim n_{\text{primary}}$, $E_k \approx mc^2 \approx 1$ MeV; then with $\omega_p = \gamma_\pm \omega_p' = 10^{10}\,\text{s}^{-1}$, $l \sim 1.5 \times 10^4$ cm and $Z \sim 10^{17}$. With such bunching the fractional efficiency for curvature radiation given in equation (47) is raised from about 10^{-13} to about 10^4. This implies that such strong bunching could cause the pair plasma to lose much of its streaming kinetic energy to curvature radiation in a very short distance, $10^{-4}\rho$, living a time $10^{-4}\gamma_\pm^3\omega_c^{-1}$. In the rest frame of the pair plasma, this time is $10^{-4}\gamma_\pm^2\omega_c^{-1} \approx 10^{-4}\gamma_\pm^2\omega_p^{-1} \sim 10^{-4}\gamma_\pm(\omega_p')^{-1}$ since the frequency of the relevant plasma mode transforms under Lorentz transformations like that of a photon moving in the direction of the plasma stream. Since $\gamma_\pm \sim 10^3$, the time in the plasma rest system during which the strong bunching need subsist for strong coherent curvature radiation is considerably less than $(\omega_p')^{-1}$. Dissipation of this plasma mode energy takes much longer than $(\omega_p')^{-1}$. Therefore, the strong two-stream coupling is expected to result in a high efficiency for the conversion of the pair plasma's streaming kinetic energy to curvature radiation at radio frequencies.

IX. PROPERTIES OF PULSAR RADIATION: THEORY AND OBSERVATIONS

a) Intensity

It follows from the argument of § VIII that a considerable fraction of gap-produced positron energy will ultimately be radiated away as curvature radiation. The maximum positron energy flux is given by equation (26). Then for pulsar radio emission intensities

$$L_{\text{radio}} < L_{\text{max}} = \frac{10^{30}}{P^{15/7}}\ \text{ergs s}^{-1} ,$$

where P is in seconds—a result which, as mentioned in § V, is not inconsistent with estimates for coherent radio emission (Cavallo 1972).

b) Spectrum of Pulsar Radio Emission

The precise frequency regime and other detailed pulsar radio emission properties depend upon a geometrical and quantitative description of the emitting region to which we now turn.

Far above the polar cap, the radius of curvature of the predominantly dipolar field lines that originate near the pole is

$$\rho = 4r^2/(3x) , \tag{58}$$

where r is the distance from the neutron star and x is the distance perpendicular to the dipole axis. Thus the angular frequency of the curvature radiation from the electrons and positrons moving along a field line that passes through (x, r) is

$$\omega_c = \frac{3}{2}\gamma_\pm^3\frac{c}{\rho} = \frac{9}{8}\gamma_\pm^3\frac{xc}{r^2} . \tag{59}$$

The pairs are produced on and travel along only the open field lines, for which (eq. [4])

$$x^2 \le \left(\frac{2}{3}\right)^{3/2}\frac{\Omega r^3}{c} . \tag{60}$$

Strong coherent radiation occurs for $\omega_c \ge \omega_p$ [the intensity of curvature radiation decreases below ω_c only as $(\omega/\omega_c)^{1/3}$]. When this criterion is combined with eqs. (52) and (59), the radiating region has an interior boundary (see fig. 8) defined by

$$x \ge \frac{16}{9\gamma_\pm^3 c}\left(\frac{2\gamma_{\text{max}} e\Omega BR^3}{mc}\right)^{1/2} r^{1/2} . \tag{61}$$

This, together with equation (60), completely specifies the radiating region. The minimum distance from the star for which coherent curvature radiation is possible

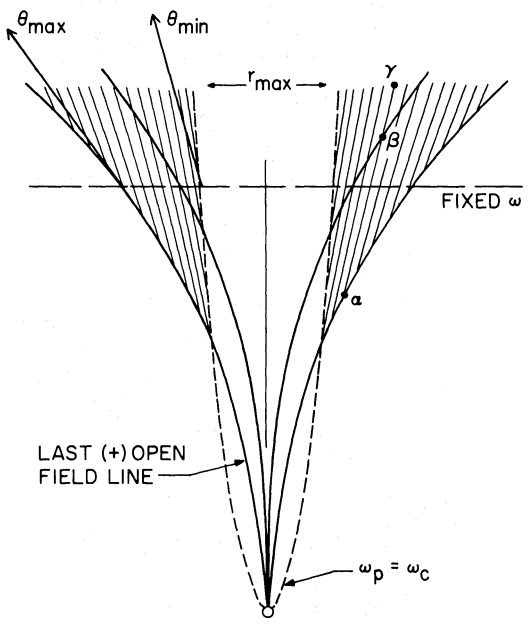

FIG. 8.—The region of coherent microwave radiation. Electrons and positrons move out along the open magnetic field lines. The bunching instability of frequency ω_p (as defined in the text) excited by the primary positrons is strongly coupled to curvature radiation outside the dashed line $\omega_p = \omega_c$; the bunching may persist out to r_{max}. Radiation of frequency ω is produced at a distance from the star given by eq. (64): $\omega \propto r^{-3/2}$. The straight lines pointing toward the neutron star are the loci of constant tangent (to the magnetic field lines) direction. Thus, electrons and positrons at the points α, β, γ radiate in the same direction but at respectively lower frequencies.

is obtained by using equations (60) and (61) as equalities:

$$r_{\min} = \frac{16}{9}\left(\frac{3}{2}\right)^{3/4}\frac{1}{\gamma_{\pm}^{3}c}\left(\frac{2\gamma_{\max}eBR^{3}}{m}\right)^{1/2} \approx 10^{8}\ \text{cm} \quad (62)$$

with the previously designated parameters.

The curvature radiation from the electrons and positrons is emitted nearly tangentially (within a cone of angle $\sim 1/\gamma_{\pm}$) to the magnetic field lines. Thus the radiation pattern and pulse envelope will be determined by the tangents to the open field lines at the points from which radiation of a given frequency may originate and by the relationship of these tangents to the direction to the observer. A dipole field line passing through (x, r) has a tangent at that point that makes an angle

$$\theta = 3x/2r \quad (63)$$

with the dipole axis. With the assumption that radiation occurs only at the local "plasma" frequency ω_p given by equation (52), the radiation at frequency $\omega = \omega_p$ originates at a distance r from the neutron star given by

$$r = 2\left(\frac{\gamma_{\max}e\Omega BR^{3}}{mc}\right)^{1/3}\omega^{-2/3}. \quad (64)$$

Equations (60) and (61) delineate the radiating region; expressed in terms of the angles made by the tangents to the field lines, and hence by the direction of the radiation, we have

$$\theta_{\min} \leq \theta \leq \theta_{\max}, \quad (65a)$$

$$\theta_{\min} = \frac{8}{3}\frac{1}{\gamma_{\pm}^{3}c}\left(\frac{\gamma_{\max}e\Omega BR^{3}}{mc}\right)^{1/3}\omega^{1/3}, \quad (65b)$$

$$\theta_{\max} = \left(\frac{3}{2}\right)^{1/4}\left(\frac{2\Omega}{c}\right)^{1/2}\left(\frac{\gamma_{\max}e\Omega BR^{3}}{mc}\right)^{1/6}\omega^{-1/3}. \quad (65c)$$

If the specific dependence of $\gamma_{\max}$ on B, ρ_s (the radius of curvature of magnetic field lines in the polar gaps), and P is included (see equation [23]), then

$$\theta_{\min} = 16^{\circ}P^{19/21}\left(\frac{B}{10^{12}}\right)^{11/17}\left(\frac{\rho_s}{10^{6}}\right)^{-15/7} \times \left(\frac{\omega}{1.0\times 10^{10}}\right)^{1/3}, \quad (66a)$$

$$\theta_{\max} = 16^{\circ}P^{-29/42}\left(\frac{B}{10^{12}}\right)^{1/7}\left(\frac{\rho_s}{10^{6}}\right)^{2/21} \times \left(\frac{\omega}{1.0\times 10^{10}}\right)^{-1/3}. \quad (66b)$$

The cone angle at which the inner and outer boundaries to the radiating region intersect (corresponding to $r = r_{\min}$; see fig. 8) is 16° for $P = 1$ s, and the radiation from that point has $\omega = \omega_{\max} = 1.0 \times 10^{10}\ \text{s}^{-1}$ and $\lambda = \lambda_{\min} = 20$ cm. In general, radiation of the highest frequency originates here, and this frequency is given by

$$\nu_{\max} = 2\times 10^{9}P^{-67/28}\left(\frac{B}{10^{12}}\right)^{-15/7}\left(\frac{\rho_s}{10^{6}}\right)^{47/14}\ \text{Hz}. \quad (67)$$

The prediction of equation (67) that $\nu_{\max} \approx P^{-67/28}$ is not strongly supported by pulsar radio spectra (see, for example, Smith 1972), although it is generally true that slower pulsars have lower high-frequency "cutoffs." (In addition to the problem of defining $\nu_{\max}$ observationally, eq. [67] depends sensitively on unknown surface parameters B and ρ_s. The region emitting radiation near $\nu_{\max}$ is also small in size and may be expected to emit very little radiation.) A prediction from this model for the low-frequency cutoff for the spectrum of a radio pulsar is even less definite. The generation of coherent radiation depends upon bunching induced in the electron-positron plasma by a beam of more relativistic primary positrons. These primary positrons move faster than the secondary electrons and positrons by essentially a speed $\Delta v = c(2\gamma_{\pm}^{2})^{-1}$, but originate in the later phases of a gap discharge, perhaps an average time Δt after the most energetic positrons of $\Delta t \approx hc^{-1}$. This means that the bunching instability may continue to be excited out to distances

$$r_{\max} \sim \frac{c^{2}}{\Delta v}\Delta t \sim 6\times 10^{9}\ \text{cm}. \quad (68a)$$

From equation (64), the frequency of the coherent radiation at this distance is

$$\nu_{\min} \sim 1.5\times 10^{7}\ \text{Hz}. \quad (68b)$$

Whether this estimate of $\nu_{\min}$ is useful depends on quantitative details of the time history of a gap discharge and on further details of the coherent radiation efficiency (for example, how much pair plasma streaming energy is left at $r \approx 6\times 10^{9}$ cm). However, the existence of a $\nu_{\min}$ in this regime does predict that pulsar radiation emission should reach a maximum at a frequency $\bar{\nu}$:

$$10^{7}\ \text{Hz} < \bar{\nu} < 2\times 10^{9}P^{-67/28}\ \text{Hz} \quad (69)$$

(with P in seconds).

c) *Integrated Pulse Envelopes: Shapes, Width, Frequency, and Period Dependence*

The structure of pulse envelopes is determined both by the direction to the observer and by the geometry of the radiating region. Radiation at frequency ω originates mostly at a distance r given by equation (64). The tangents to the field lines at this level define various radiation cones (see fig. 9*a*). If the dipole axis is not parallel to the rotation axis, then, as the radiation cones sweep by the direction to the observer, a line (the observer's "trajectory") is defined across the common "base" of these cones such that the observer receives radiation only from points on this line. The family of nested radiation cones has an inner cone defined by $\theta_{\min}(\omega)$ interior to which no radiation of

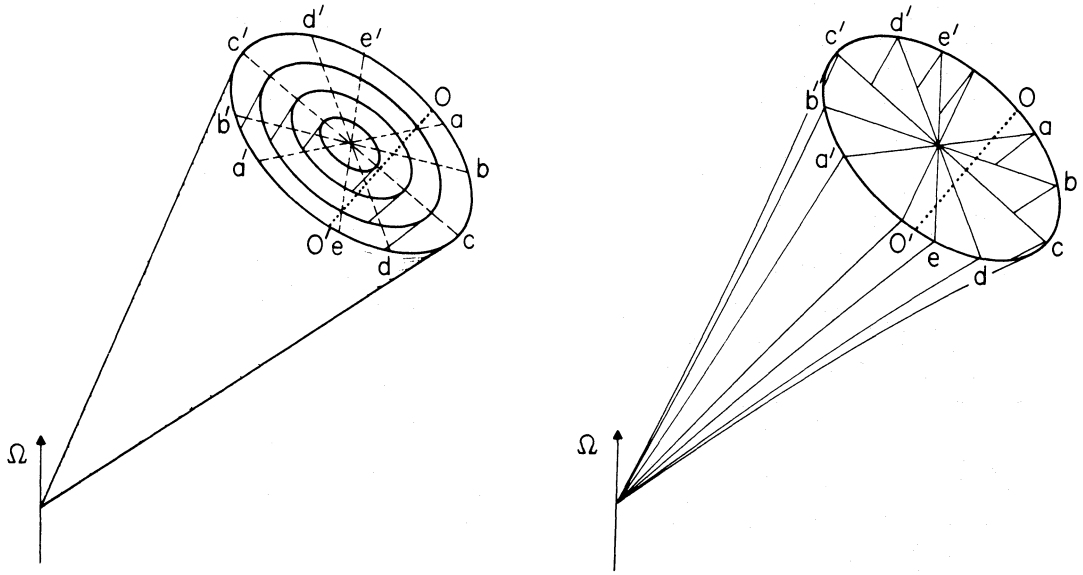

FIG. 9*a* (*left*).—Representation of the radiation cones for a given frequency ω defined by the tangents to the magnetic field lines, at a distance from the star given by eq. (64). These cones are symmetric about the magnetic dipole axis which is inclined with respect to the rotation axis. The sweeping of the cone past the direction to the observer defines an observer's path OO' relative to the cones: the observer receives radiation at frequency ω only from emission angles defined by the intersection of OO' and these cones.

FIG. 9*b* (right).—Representation of the planes of the curved dipole magnetic field lines of the radiating region. The curvature radiation from particles streaming along the field lines has strong linear polarization with the electric vector in the plane of curvature. As the direction to the observer moves, relative to the radiating region, along OO' the position angle sweeps continuously from that of the plane aa' to that of the plane ee'.

frequency ω originates and an outer cone defined by $\theta_{max}(\omega)$ exterior to which no radiation originates. The pulse envelope is determined by the observer's "trajectory"; and if this line passes inside of $\theta_{min}(\omega)$, an observer sees a double-humped envelope. If not, only a single-humped envelope should be seen (see fig. 10). Since $\theta_{min}(\omega)$ and $\theta_{max}(\omega)$ are only weak functions of ω, this distinction between one-humped and two-humped envelopes should be present at all frequencies, although it is expected that for two-humped envelopes, at the higher frequencies, the humps should be narrower and somewhat closer together. The calculated separation, from equation (66b), is proportional to $\omega^{-1/3}$. This appears to be compatible with many of the observations of Lyne, Smith, and Graham (1971).

Because $\theta_{min} \approx P^{19/21}$, the observer's "trajectory" is more likely to go inside θ_{min} in the long-period pulsars: one therefore expects these pulsars to have a preponderance of double-humped envelopes. Long-period pulsars need not, of course, have double-humped envelopes provided the observer's "trajectory" does not pass through θ_{min}; but then long-period pulsars with single-humped envelopes should have especially narrow envelopes. Similarly, short-period pulsars may have double-humped envelopes in the rare case when the observer's "trajectory" goes very near the polar axis. When this happens, the full width of the envelope should also be relatively large. These qualitative remarks seem to be borne out by the collection of sample envelopes of Smith (1972). The dependence of θ_{max} on period, $\theta_{max} \approx P^{-29/42}$, appears to be

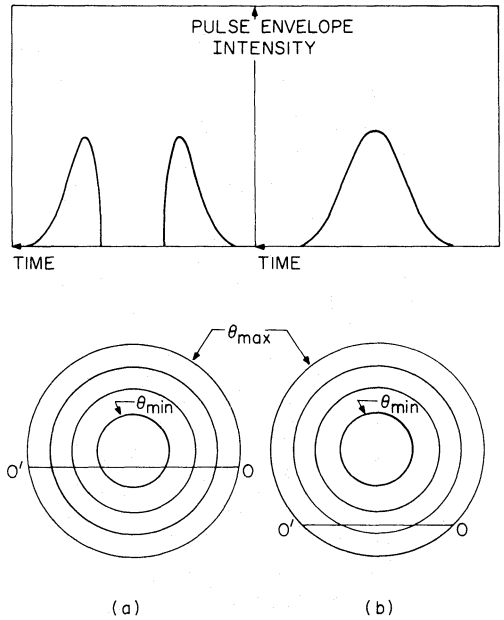

FIG. 10.—Schematic representation of the origins of double-humped and single-humped pulse envelopes. The angles of the radiation cones are defined by the tangents to the magnetic field lines: interior to θ_{min} there is no coherent microwave radiation; θ_{max} is determined by the tangents to the last open field lines. When the direction to the observer defines a path OO' relative to these cones that passes interior to θ_{min}, a double-humped envelope results. The angle θ_{min} increases with period, roughly as P so that a preponderance of double-humped envelopes is expected for the longer-period pulsars but can occur for certain OO' trajectories even for short-period pulsars.

stronger than that suggested by analyses of pulse widths: $\theta_{\rm width} \sim P^{-0.3}$ (Gunn and Ostriker 1970; Roberts and Sturrock 1972, 1973). However, the direct relation of $\theta_{\rm max}$ to the observed pulse width is somewhat clouded by two considerations: (i) although coherent radiation from any field line starts when $\omega_c > \omega_p$, just how far beyond this point it continues strongly, and whether it extends all the way to $\theta_{\rm max}$, depends upon the detailed time history of gap particle production and how quickly and strongly bunching develops; (ii) observationally, pulse widths may vary considerably with the shape of the envelope and the fractional power level at which they are defined.

d) Polarization

In a "typical" pulsar, the radio radiation has strong linear polarization whose direction sweeps smoothly over a large range through the pulse, often as much as 180° (see Manchester 1971). As pointed out by Radhakrishnan and Cooke (1969) and others, this phenomenon follows naturally in models similar to the one considered here: Curvature radiation is emitted tangentially to the magnetic field lines with an electric polarization vector in the plane defined by that curved field line whose electrons give the curvature radiation observed at that instant. Since the open dipole field lines originate on and diverge away from the polar cap, the planes defined by their curvature intersect the observer's trajectory as indicated in figure 9*b* and give an observed swing of the polarization. In this picture, if a pulsar has an anomalously narrow envelope, then one expects the swing of polarization to be correspondingly smaller. This seems to be supported by the observations (Manchester 1971).

We note finally that essentially all of the radio radiation of typical pulsars is predicted to occur at distances of order 10^2 stellar radii above the polar caps. At such distances, magnetic field irregularities which may be important within the polar gap or within 10^6 cm of the stellar surface are expected to be absent, and a pure dipole field approximation may be reasonable. (Many of our estimates have depended only upon the total magnetic flux in this field component.) The great complexity of some pulse envelopes must then be attributed to the nonuniform injection from the spark pattern in the polar gap. This pattern may also drift, as discussed in § VI, or even change suddenly. Polarization angles may also be complex when radiation comes from a few bunches and pencils rather than uniformly from throughout the emitting region. More realistic models with nonaligned magnetic moments have twisted open field lines swept back by the rotation. In such cases the polarization is more complicated and may depend upon the injection pattern. This will be discussed in detail elsewhere.

It is a pleasure to thank Professors R. M. Manchester and M. N. Rosenbluth for helpful and illuminating conversations.

APPENDIX

EXACT RESULTS FOR SIMPLE GAPS

In this Appendix we present some exact results for simple model gaps and discuss a general theorem on axisymmetric magnetospheres.

I. SPHERICAL GAP

We consider a rotating (angular frequency Ω^*) neutron star with an axisymmetric dipolar magnetic field aligned with the rotation axis (cf. fig. 1). For simplicity, we assume that the neutron star is uniformly magnetized with a magnetization $\boldsymbol{M} = (\frac{3}{8}\pi^{-1}B_p)\hat{z}$, where z is the common direction of the rotation and dipole axes and B_p is the polar magnetic field strength on the surface [B_p is positive (negative) if the rotation and dipole axes are parallel (antiparallel)]. Within the neutron star the matter is assumed to be a conductor. Because of the interior uniform aximagnetization, the interior electric field and charge density are given by

$$\boldsymbol{E}^{(\rm in)} = -\frac{B_p\Omega^* r_\perp}{c}\hat{e}_\perp\,, \quad \rho_e = \frac{\nabla\cdot\boldsymbol{E}}{4\pi} = -\frac{B_p\Omega^*}{2\pi c}\,, \tag{A1}$$

where $r_\perp = r\sin\theta$ is the cylindrical coordinate perpendicular to the rotation axis. A corotating perfectly conducting magnetosphere has an electric field and charge density that ensure corotation:

$$\boldsymbol{E}^{(\rm out)} = -\frac{(\boldsymbol{\Omega}^* \times \boldsymbol{r}) \times \boldsymbol{B}}{c}\,, \quad \rho_e = -\frac{\boldsymbol{B}\cdot\boldsymbol{\Omega}^*}{2\pi c}\,. \tag{A2}$$

For an aligned dipolar magnetic field the magnetosphere charge density is purely quadrupolar. [The above results are correct to order $(v/c)^2$ and hence only valid "near" the neutron star—within some radius $\tilde{R} \ll c/\Omega$. The departure of the magnetic field from a strictly dipolar form is determined by the Maxwell equation $\nabla\cdot\boldsymbol{B} = 4\pi\boldsymbol{J}/c = 4\pi\rho_e(\boldsymbol{\Omega}^* \times \boldsymbol{r})/c$ and is $O(v^2/c^2)$; the lowest-order corrections may be included but are essentially irrelevant to the

discussion which follows and will consequently be ignored.] With the exterior and interior electric fields determined by equations (A1) and (A2), the surface charge density on the neutron star is

$$\sigma_e = \frac{(\boldsymbol{E}^{(\text{out})} - \boldsymbol{E}^{(\text{in})})\cdot\hat{n}}{4\pi} = \frac{3}{2}\frac{B_p\Omega^* R}{4\pi c}(1 - \cos^2\theta)\,. \tag{A3}$$

It clearly has both a quadrupole and a monopole component. The total charge of the neutron star as determined by equations (A1) and (A3) is $Q = \frac{1}{3}B_p\Omega^* R^3/c$; this can, of course, be directly verified by computing the surface integral $\frac{1}{4}\pi^{-1}\oint \boldsymbol{E}^{(\text{out})}\cdot d\boldsymbol{A}$ over any sphere concentric with the neutron star. (The volume and surface charge densities determined above may be further analyzed in terms of their "physical" components—free space charge and polarization charge—but this separation is not important to the following discussion.)

We now proceed to the case where the magnetosphere has a gap. This gap, or vacuum, is a spherical shell extending from the neutron star surface to a height h; the electric field in this gap must satisfy $\nabla\cdot\boldsymbol{E} = 0$. Because the stellar surface can retain charge, $\boldsymbol{E}\cdot\boldsymbol{B}$ need not vanish there; but it must at the upper gap boundary with the magnetosphere. We anticipate that the magnetosphere is not corotating at the angular velocity Ω^* of the neutron star, but at a different angular velocity Ω. The interior charge density of the neutron star is monopolar and determined by Ω^*; the monopolar component of the surface charge is determined by the requirement that the magnetosphere rotate at angular velocity Ω—the net charge of the neutron star must be $\frac{1}{3}B_p\Omega R^3/c$. There remain two undetermined quantities: the amplitude of the surface charge quadrupole moment and the relationship of Ω to Ω^* and h. These may be obtained as follows. The interior of the neutron star "sees" an exterior quadrupole charge distribution from the surface quadrupolar charge distribution and the magnetosphere. The field determined by these must combine with the electric field from the interior charge monopole to give a net electric field $\boldsymbol{E}^{(\text{in})} = -(B_p\Omega^* r_\perp/c)\hat{e}_\perp$. In the absence of a gap, the magnetosphere exterior to $R' = R + h$ "sees" a quadrupole moment $-\frac{1}{5}(B_p\Omega/c)R^3R'^2$; with a gap extending to height h, this quadrupole moment must now be reproduced entirely by the surface quadrupole moment. These two conditions lead to a complete specification for the neutron star and magnetosphere.

a) Neutron Star

$$\text{Interior charge density:}\quad \rho_e^{(\text{in})} = -\frac{\Omega^* B_p}{2\pi c}\,.$$

$$\text{Surface charge density:}\quad \sigma = \sigma_0 + \sigma_2 P_2(\cos\theta)\,, \tag{A4}$$

$$\sigma_0 = \frac{1}{3}\frac{B_p R}{4\pi c}(2\Omega^* + \Omega)\,,$$

$$\sigma_2 = -\frac{1}{4\pi}\frac{B_p\Omega}{c}\frac{(R+h)^2}{R}\,.$$

b) Magnetosphere

$$\rho^{(\text{out})} = -\frac{B_p\Omega}{2\pi c}\left(\frac{R}{r}\right)^3 P_2(\cos\theta) \tag{A5}$$

and

$$\frac{\Omega^*}{\Omega} = \frac{3}{5}\frac{(R+h)^2}{R^2}\left[1 + \frac{2}{3}\frac{R^5}{(R+h)^5}\right] \tag{A6}$$

$$= 1 + 3h^2/R^2 \qquad \text{for } h \ll R.$$

The potential difference between a point on the stellar surface and one above it at the top of the gap is

$$\Delta V = \left(\frac{\Omega B_p R^3}{3c}\right)\left\{P_2(\cos\theta)\left[\frac{2}{5}\frac{R^2}{(R+h)^3} + \frac{3}{5}\frac{(R+h)^2}{R^3} - \frac{1}{R+h}\right] - \frac{h}{R(R+h)}\right\}. \tag{A7a}$$

The electric field (E_s) is normal to the surface at the poles and vanishes at the top of the gap. In the $h \ll R$ regime,

$$E_s = -\frac{2\Omega B_p h}{c}\,, \qquad \Delta V = \frac{\Omega B_p h^2}{c}\,. \tag{A7b, c}$$

The relations (A7) hold for any sufficiently narrow gap ($h \ll R$) no matter what the multipolarity of the stellar magnetic field.

II. INFINITESIMAL POLAR GAP

In the pulsar model of this paper, a gap develops in the polar regions because of the inability of the surface to replenish the positive ions that drift out of the magnetosphere along the open field lines. In this subsection we consider the characteristics of such a gap when the gap thickness becomes small compared with the base radius r_p of the gap. If it is small, the relations (A7b, c) hold except near the edge. We consider the limit $h \ll r_p \ll R$ so that the neutron star surface may be idealized as flat and the magnetic field lines as vertical. The solution has not been given analytically but is sketched in figure 2. A magnetosphere column separated by h from the stellar surface also separates by this same distance h from its cylindrical side boundary. It is as if a uniform *negative* charge density $-\Omega B(2\pi c)^{-1}$ is put into the gap to cancel the usual magnetospheric positive charge there. At the stellar surface, the electric field components perpendicular to $\boldsymbol{B}$ are unchanged and thus, in terms of the departures of the electric field and potential from their zero-gap values, the stellar surface acts like an equipotential boundary. Thus the outer surfaces bounding the gap act just like a conducting surface. The inner surfaces satisfy $\Delta \boldsymbol{E}\cdot\boldsymbol{B} = 0$ everywhere. In the limit $h \ll r_p \ll R$ the geometry is rectangular and the region above a "corner" is similar to one on the surface side.

III. INFINITE POLAR GAP

Here we have $h \gg r_p$ and we make the assumption $h \ll R$: such limits will be attained for very slowly rotating neutron stars since $r_p \sim R(R\Omega/c)^{1/2}$. Then we may again approximate the stellar surface as flat and the magnetic field lines as normal to the surface. The geometry is cylindrical: we have axisymmetry and work with cylindrical coordinates $(r_\perp, \phi, z)$. Below the surface of the neutron star the electric field is $E_\perp = \Omega B r_\perp/c$ (the magnetic field is vertical and constant: $\boldsymbol{B} = -B\hat{z}$); for $r_\perp \geq r_p$ the magnetosphere is corotating at angular velocity Ω while interior to r_p there is a complete vacuum. In the gap, the potential is a solution of Poisson's equation and takes the form

$$V(z, r_\perp) = \sum_{i=1}^{\infty} a_i \exp(-x_{0i} z/r_p) J_0(x_{0i} r_\perp/r_p), \tag{A8}$$

where the x_{0i} are zeros of the zeroth-order Bessel function J_0. This potential satisfies the requirement that the magnetic field lines that constitute the gap boundary are equipotentials. The coefficients a_i are determined by the requirement that $E_\perp$ be continuous across the neutron star surface, or equivalently that

$$V(0, r_\perp) = \Omega B(r_p^2 - r_\perp^2)/2c; \tag{A9}$$

thus

$$a_i = \frac{2}{[r_p J_1(x_{0i})]^2} \int_0^{r_p} dr_\perp r_\perp V(0, r_\perp) J_0(x_{0i} r_\perp/r_p) = 2\frac{B\Omega r_p^2}{c}\frac{J_2(x_{0i})}{x_{0i}^2}. \tag{A10}$$

The vertical potential difference of the gap is simply

$$\Delta V(r_\perp) \equiv V(0, r_\perp) = \tfrac{1}{2} B\Omega(r_p^2 - r_\perp^2)/c, \tag{A11}$$

and has its maximum at the center.

The essential characteristics of this simple model gap are that the potential and electric field have a vertical scale height of order r_p and that the maximum vertical potential difference is $\frac{1}{2}B\Omega r_p^2/c$. Thus, for $h \gg r_p$ the formulae that apply in the $h \ll r_p$ case remain valid with the substitution $h \to r_p/\sqrt{2}$.

IV. A THEOREM ON MAGNETOSPHERES

Consider a rotating neutron star with an axisymmetric magnetic field. If the neutron star has a magnetosphere, then in those regions of the magnetosphere for which $\boldsymbol{E}\cdot\boldsymbol{B} = 0$ (i.e., no particle acceleration along these field lines) the following are true:

a) Such regions are corotating in the sense that within the magnetospheric plasma there is an electric field given by

$$\boldsymbol{E} = -\frac{(\boldsymbol{\Omega} \times \boldsymbol{r}) \times \boldsymbol{B}}{c}, \tag{A12}$$

and this results in a drift velocity corresponding to rotation at angular velocity $\boldsymbol{\Omega} = \Omega\hat{z}$; Ω is in general a function of the cylindrical coordinates $r_\perp$ and z.

b) Ω is constant along magnetic field lines:

$$B_\perp \frac{\partial \Omega}{\partial r_\perp} + B_z \frac{\partial \Omega}{\partial z} = 0. \tag{A13}$$

Thus for magnetospheric regions connected to the neutron star by magnetic field lines all along which $\boldsymbol{E}\cdot\boldsymbol{B}$ vanishes, the corotation angular velocity is that of the neutron star itself. This is Ferraro's theorem (see, for example,

Alfvén and Fälthammer 1963). As a corollary to the theorem, we note that the charge density within such a magnetosphere is

$$\rho_e = \frac{1}{4\pi[1 - (\Omega r_\perp/c)^2]}\left[-2\boldsymbol{\Omega}\cdot\boldsymbol{B} + r_\perp\left(-B_z\frac{\partial\Omega}{\partial r_\perp} + B_\perp\frac{\partial\Omega}{\partial z}\right)\right]. \quad \text{(A14)}$$

REFERENCES

Alfvén, H., and Fälthammer, C.-G. 1963, *Cosmical Electrodynamics* (London: Oxford University Press), p. 110.
Backer, D. C. 1973, *Ap. J.*, **182**, 245.
Baym, G., Pethick, C., and Sutherland, P. 1971, *Ap. J.*, **170**, 299.
Bludman, S. A., Watson, K. M., and Rosenbluth, M. N. 1960, *Phys. Fluids*, **3**, 747.
Boynton, P. E., Groth, E. J., Hutchinson, D. P., Nanos, G. P., Jr., Partridge, R. B., and Wilkinson, D. T. 1972, *Ap. J.*, **175**, 217.
Cavallo, G. 1972, *Astr. and Ap.*, **18**, 287.
Chen, H.-H., Ruderman, M. A., and Sutherland, P. G. 1974, *Ap. J.*, **191**, 473.
Erber, T. 1966, *Rev. Mod. Phys.*, **38**, 626.
Gold, T. 1959, *J. Geophys. Res.*, **61**, 1219.
Goldreich, P., and Julian, W. H. 1969, *Ap. J.*, **157**, 869.
Greenstein, G. 1971, *Nature Phys. Sci.*, **232**, 117.
———. 1972, *Ap. J.*, **177**, 251.
Gunn, J. E., and Ostriker, J. P. 1970, *Ap. J.*, **160**, 979.
Hankins, T. H. 1971, *Ap. J.*, **169**, 487.
Kuo-Petravic, L. G., Petravic, M., and Roberts, K. V. 1974, *Phys. Rev. Letters*, **32**, 1019.
Lyne, A. G., Smith, F. G., and Graham, D. A. 1971, *M.N.R.A.S.*, **153**, 337.
Manchester, R. N. 1971, *Ap. J. Suppl.*, **23**, 283.
Manchester, R. N., Tademaru, E., Taylor, J. H., and Huguenin, G. R. 1973, *Ap. J.*, **185**, 951.
Michel, F. C. 1974, *Ap. J.*, **192**, 713.
Prentice, A. J. R., and ter Haar, D. 1969, *M.N.R.A.S.*, **146**, 423.
Radhakrishnan, V., and Cooke, D. J. 1969, *Ap. Letters*, **3**, 225.
Roberts, D. H., and Sturrock, P. A. 1972, *Ap. J.*, **172**, 435.
———. 1973, *ibid.*, **181**, 161.
Rosen, L. C., and Cameron, A. G. W. 1972, *Ap. and Sp. Sci.*, **15**, 137.
Ruderman, M. A. 1972*a*, *Ann. Rev. Astr. and Ap.*, **10**, 427.
———. 1972*b*, *IAU Symposium 53, The Physics of Dense Matter* (*Boulder, Colo.*), ed. S. Tsuruta (to be published).
Smith, F. G. 1972, *Rept. Progr. Phys.*, **36**, 399.
Sturrock, P. A. 1971, *Ap. J.*, **164**, 529.
Sturrock, P. A. 1971, *Ap. J.*, **164**, 229.
Tademaru, E. 1971, *Ap. and Space Sci.*, **12**, 193.
Taylor, J. H., and Huguenin, G. R. 1971, *Ap. J.*, **167**, 273.
ter Haar, D. 1972, *Phys. Report*, **3C**, 58.
Terzian, Y. 1973, Pulsar Data Sheet (unpublished).
Tsuruta, S., Canuto, V., Lodenquai, J., and Ruderman, M. A. 1972, *Ap. J.*, **176**, 739.

Note added in proof.—Holloway (*Nature Phys. Sci.*, **246**, 6 [1973]) has considered the development of similar gaps at the boundaries separating the positive and negative regions of the magnetosphere.

M. A. RUDERMAN: Dept. of Physics, Columbia University, New York, NY 10027

P. G. SUTHERLAND: Dept. of Physics, University of Pennsylvania, Philadelphia, PA 19174